

University of Mississippi

eGrove

Electronic Theses and Dissertations

Graduate School

1-1-2023

Action in Causal Set Theory

Santosh Bhandari

University of Mississippi

Follow this and additional works at: <https://egrove.olemiss.edu/etd>

Recommended Citation

Bhandari, Santosh, "Action in Causal Set Theory" (2023). *Electronic Theses and Dissertations*. 2661.
<https://egrove.olemiss.edu/etd/2661>

This Thesis is brought to you for free and open access by the Graduate School at eGrove. It has been accepted for inclusion in Electronic Theses and Dissertations by an authorized administrator of eGrove. For more information, please contact egrove@olemiss.edu.

ACTION IN CAUSAL SET THEORY

A thesis
presented in partial fulfillment of requirements
for the degree of Master of Science
in the Department of Physics and Astronomy
The University of Mississippi

by

SANTOSH BHANDARI

August 2023

Copyright Santosh Bhandari 2023
ALL RIGHTS RESERVED

ABSTRACT

The aim of this thesis is to explore causal set theory (CST), which proposes that at the smallest level of spacetime, discrete entities known as “spacetime atoms” are causally related to one another, forming the basis for understanding quantum gravity. While theories such as general relativity that operate on a continuous manifold are more appropriate when dealing with the universe on a large scale, it is crucial for the discrete causal points in CST to maintain their causal structure during the continuum approximation to ensure consistency with general relativity. One way to preserve the causal structure is to accurately embed the set of causally discrete points (known as a causal set) into a Lorentzian manifold, resulting in manifoldlike causal sets. The thesis will investigate the dynamics of manifoldlike causal sets through two distinct approaches to calculating action: layers and chain. The layer action, known as the Benincasa-Dowker action, introduces a discrete non-local operator, which is represented as a linear combination of various layer elements, aims to find the solution for the action. On the other hand, the chain action explores the distribution of k -chains to determine the action. The thesis will explore potential enhancements to the existing chain action calculation, particularly by incorporating higher-order terms of scalar curvature in the derivation.

ACKNOWLEDGEMENTS

I would like to sincerely thank Dr. Luca Bombelli, my research mentor, for his unwavering support and guidance throughout my research journey. Dr. Bombelli not only recognized my passion for quantum gravity but also provided me with numerous opportunities to expand my knowledge and skills. This experience has been incredibly valuable and has enriched my understanding. Furthermore, I am grateful to Dr. Benjamin Pilgrim and graduate student He Liu for their valuable contributions to my research. Their insights have greatly influenced my work. I would also like to appreciate Ayush Dhital, Nauman Ibrahim, and Irby Coleman for their invaluable feedback and insightful suggestions during the research process. Their input has been instrumental in shaping my work. Finally, I extend my heartfelt thanks to my friends Azwad Adnan and Anil Panta for their invaluable assistance during my research endeavors.

TABLE OF CONTENTS

ABSTRACT	ii
ACKNOWLEDGEMENTS	iii
LIST OF FIGURES	v
CHAPTER 1: INTRODUCTION	1
1.1 Birth of Quantum Gravity	1
1.2 A Promising History Behind Causal Sets Theory	4
1.3 Causal Set Hypothesis	5
1.3.1 Definition	5
1.3.2 Continuum Approximation	7
CHAPTER 2: BENINCASA-DOWKER ACTION FOR CAUSAL SET	10
2.1 Non-Locality in CST and Quasi-local operator	10
2.2 Action using the Benincasa-Dowker Method	13
CHAPTER 3: CHAIN ACTION FOR CAUSAL SET	21
3.1 Chain Length Distribution	22
3.2 Chain length distribution in Minkowski spacetime	23
3.3 Chain length distribution in Curved spacetime	26
3.4 Chain Action	31
CHAPTER 4: HIGHER ORDER CORRECTION FOR CHAIN ACTION	34
4.1 $\langle C_3 \rangle$ including higher-order correction	37
4.2 $\langle C_4 \rangle$ including higher-order correction	38
4.3 Chain Action with higher-order correction	39
CONCLUSION	41
LIST OF REFERENCES	43
APPENDICES	45
VITA	50

LIST OF FIGURES

1.1	Hasse Diagram	6
1.2	KR-Figure	8
1.3	Manifoldlike causal sets sprinkled in the minkowski spacetime of 1000 elements	9
1.4	Manifoldlike causal sets sprinkled in the de Sitter spacetime of 1000 elements	9
2.1	Locality problem in CST	11
2.2	Layers in CST	12
2.3	Partition of W into regions W_1, W_2, W_3 in $t - r$ plane	16
2.4	Plot of the Benincasa-dowker action vs number of sprinkled points in minkowski spacetime	19
2.5	Plot of the Benincasa-dowker action vs number of sprinkled points in de Sitter spacetime	19
3.1	Illustration of a chain of length k and two examples to showcase how the distribution of points affects the total number of chain length k	21
3.2	Distribution of k -chain abundance as a function of k -chain length for Minkowski and de Sitter spacetime.	22
3.3	Visual representation by which chains are obtained	23
3.4	Visual representation of region of intergation for $\langle C_3 \rangle$ and $\langle C_4 \rangle$	24
3.5	Verification of expectation value of k-chain formulae with the simulation in minkowski spacetime using $k= 3, 4$	26
3.6	Verification of expectation value of k=chains formulae with the simulation data in de Sitter spacetime	30
3.7	Chain action for minkowski spacetime	32
3.8	Chain action for de Sitter spacetime for 3-chains and 4-chains with $H = 100$ and $\rho = 2000000$	32

3.9	Chain action for de Sitter spacetime for $H = 50$ and $\varrho = 2000000$	33
4.1	Causal set action S when higher order term of scalar curvature is considered	39
4.2	Chain action comparison	40
A.1	Causal diamond inside a square lorentzian manifold	46

CHAPTER 1

INTRODUCTION

1.1 Birth of Quantum Gravity

Gravity, one of the earliest observed phenomena in the universe, remains one of the least understood to this day. Einstein's groundbreaking work, "The Foundation of General Theory of Relativity," published in 1915, presents the most consistent theory of gravity in accordance with the experimental observations and is widely accepted by many physicists in the present era. According to this theory, gravity is the manifestation of the curvature of spacetime. The paths of objects are determined by the curvature of spacetime. The spacetime is described as a Lorentzian manifold endowed with a metric tensor. The field equation governing the evolution of the metric is given by:

$$R_{\mu\nu} - \frac{1}{2}Rg_{\mu\nu} + \Lambda g_{\mu\nu} = \frac{8\pi G}{c^3}T_{\mu\nu} \quad (1.1)$$

Here, G is Newton's gravitational constant, $R_{\mu\nu}$ and R represent the Ricci tensor and scalar respectively, $g_{\mu\nu}$ is the metric tensor, c is the speed of light, Λ represents Cosmological Constant, and $T_{\mu\nu}$ represents the energy-momentum tensor.

As referred in Ref.¹, this theory has successfully predicted phenomena such as the existence of black holes, the behavior of planets in their orbits, gravitational waves, and the bending of light due to gravity with great precision. However, despite its many successful predictions, the theory has significant limitations. It not only permits singularities but also deems them inevitable in certain real-world scenarios, necessitating a thorough comprehension of them for a complete understanding of spacetime's nature. While some physicists view the prediction of singularities as an excellent chance to explore uncharted territories and expand our knowledge of the physical world, most

believe it indicates inadequacies in the theory's ability to model such behavior. This is because they believe that our physical world does not exhibit singularities. In general relativity, singularities occur when a particle's path in spacetime becomes incomplete or unextendible, disappearing from spacetime after a finite amount of time. It's as if there's a rip in the fabric of spacetime, causing any path passing through it to fall in and vanish. If we were to ask what causes the path's incompleteness, we would have to refer to the geometry of spacetime, especially its curvature. It seems that near the singularities, the local measure of curvature seems to approach infinity, which is evident when measuring curvature near black holes. These spacetime singularities predicted by general relativity, whether attributed to path incompleteness or infinite curvature, are not physical and are leading the theory towards its own demise.

While some physicists argue that spacetime singularities are real, they remain hidden behind event horizons, making them inaccessible to external observers. General relativity also predicts unbounded "naked singularities" that are available to outside observers. One type of these singularities is the "white hole" or time-reversed black hole. Roger Penrose has stated that these objects are nonphysical and violate the laws of thermodynamics. All of these phenomena suggest that to investigate black holes or the Big Bang, one must either improve the current assumptions made in general relativity or find a replacement theory.

It is worth exploring what might have gone wrong with the theory of relativity. The theory posits that the universe can be represented as a spacetime manifold with a metric that is shaped by the distribution of matter in the spacetime. This is a classical theory that assumes physical quantities have definite positions and momenta defined by real numbers. However, the behavior of matter-energy and their interactions is inherently quantum mechanical. The classical theory can be applied at a macroscopic scale because quantum fluctuations are insignificant. However, when we try to apply it to extremely small scales, it fails because we can no longer disregard quantum effects. Therefore, to study such extreme conditions, we need a quantized theory of gravity. One method is to quantize the gravitational field similarly to how we quantize the electromagnetic field. However, this approach comes with significant challenges such as non-renormalizability and

the inability of perturbative methods. These difficulties arise because while quantizing gravity we need to consider quantum fluctuations in spacetime itself. For instance, the theory of quantum electrodynamics assumes that there is a classical background or spacetime against which all quantum fluctuations are measured. This approach makes it possible to renormalize the quantization process. However, if we tried to quantize the background/spacetime itself, it would be difficult to interpret the fluctuations of spacetime. This is because if the metric of spacetime fluctuates, it would imply fluctuations in the causal structure and ordering of events. This would then make it impossible to define equal time commutation relations in quantum field theory. Therefore, the difficulty of unifying the two essential foundations of physics, namely quantum field theory (QFT) and general relativity (GR), was realized.

Looking back at the history of physics, it becomes clear that progress in the field has always required unification of different forces. The integration of major basic forces has had a significant impact on the advancement of physics, as demonstrated by the unification of electricity and magnetism through Maxwell's equations and the integration of electromagnetism with Newtonian mechanics to develop special relativity. Dirac further unified quantum mechanics with special relativity to create quantum field theory. These successful unifications have led to the recognition of four fundamental forces of nature: strong force, weak force, electromagnetic force, and gravitational force. The continued progress in electro-weak theory and previous unification theories suggests that physics must keep striving for further unification. The remaining task is to unify the gravitational force with quantum field theory, which has led to the creation of a new field known as "Quantum Gravity".

According to David Reid, "Quantum Gravity is a theory that describes the structure of spacetime and the effects of spacetime structure down to sub-Planckian scales".

We will discuss one of many approaches to quantum gravity known as "Causal Sets Theory" in the next section.

1.2 A Promising History Behind Causal Sets Theory

One of the consequences of special relativity is the realization that space and time are not separate entities but are part of a single construct known as spacetime. By considering spacetime as a Lorentzian manifold equipped with a metric tensor, the concept of local lightcones and causal structure emerged. The spacetime interval between two events depends on the metric tensor and determines which event qualify as causal, null, or spacelike related.

$$ds^2 = g_{\mu\nu} dx^\mu dx^\nu \quad (1.2)$$

Here, $g_{\mu\nu}$ is the metric associated with the spacetime. In Lorentzian signature $(-,+,+,+)$, if the spacetime interval between two events is timelike ($ds^2 < 0$), they are causally related. On the other hand, if the spacetime interval is spacelike ($ds^2 > 0$), the two events are not causally related. The metric is used to recover the causal relationship between events, and as stated in the previous section, quantization of spacetime refers to quantization of this metric. But, what if the metric is not a fundamental property of spacetime but rather an emergent property? What if we start by considering causal relationships and calculate the metric from there? If we take causal relationships as the starting point instead of the metric, then it would mean that the quantization of spacetime would be the same as quantizing the causal structure of spacetime. This is the approach of CST, which takes the causal structure of spacetime as the starting point for quantization, rather than the metric.

To characterize the spacetime based on its causal structure, it can be represented as a partially ordered set (poset) consisting of all events or points in the spacetime along with their causal relations $(M, <)$. This is known as a continuum causal poset. The main question is whether this continuum causal poset contains the same information as the metric of the spacetime. As mentioned in Ref. ², Zeeman in 1964 demonstrated in his paper titled “Causality Implies the Lorentz group” that the Lorentz group arises naturally from the idea of causality. He showed that causal relations alone may be sufficient to recover the Lorentzian manifold. This concept was further developed by Malament

in 1977 through the Hawking-King-McCarthy-Malament theorem (HKMM).

The HKMM theorem states that: **If a causal bijection exists between two d -dimensional spacetimes which are both future and past distinguishing, then these spacetimes are conformally isometric when $d > 2$.**

In other words, if the causal structure of two spacetimes is the same, then they must also be conformally isometric, meaning that they are the same up to a conformal factor that encodes the volume of space. Therefore, the continuum causal poset carries the same information as the metric of the spacetime up to a conformal factor. However, since the continuum causal poset is uncountably infinite, it cannot represent volume. To solve this issue, we can use a discrete causal poset that is locally finite and can represent volume as the total count of its elements. The discrete causal poset just mentioned above is what we call “Causal Sets” and the theory of these causal sets is called “Causal Sets Theory”. The formal definition of CST by Bombelli et al Ref.³ is followed in the next section.

1.3 Causal Set Hypothesis

To mathematically investigate the features of spacetime in terms of its causal structure, we need to establish a framework for causal sets. The basis of this framework is formed by defining axioms for causal set theory. With the help of these axioms, we can define causal sets as:

1.3.1 Definition

A locally finite partially ordered set with an order relation ($<$) is called a causal set $(C, <)$ if it satisfies the following properties:

Anti-Reflexive: $\forall x \in C$, we have $x \not< x$.

Non-Circularity: $\forall x$ and $y \in C$, we have $x < y$ and $y < x$ implies $x = y$.

Transitive: $\forall x, y, z \in C$, we have $x < y$, and $y < z$ implies $x < z$.

Locally finite: $\forall x, z \in C$, we have $|I(x, z)| < \infty$.

Here, $x < y$ means x is in the past of y , $|\cdot|$ is the cardinality of the set, and $I(x, z) = \{y \in C \mid x < y < z\}$ is an order interval. $I(x, z)$ is a causal set analogue of the Alexandrov interval (A_0) in the continuum, where $A_0 = J^+(x) \cap J^-(z)$.

The **Anti-Reflexive** property states that no event is causally related to itself, while the **Non-circularity and Transitivity** together define C as a poset. The poset can be represented by a Hasse diagram, where the dots are elements, and the line between them is a causal relation represented in a matrix called the “Relation matrix.” The property of the elements in this matrix is described by

$$R_{ij} = \begin{cases} 1 & \text{if } i < j \\ 0 & \text{otherwise} \end{cases} \quad (1.3)$$

Let’s introduce some terminology that will be useful later.

- a) A *link* is defined as a pair of elements $a, b \in C, \implies a < *b$, and $I(a, b) = \emptyset$
- b) A *chain* is a sequence of elements $a_0, a_1, \dots, a_n, \implies a_j < a_{j+1}$ for $j = 0, 1, 2, \dots, (n-1)$.
- c) If every a_j, a_{j+1} forms a link, then the chain is called a *path*.

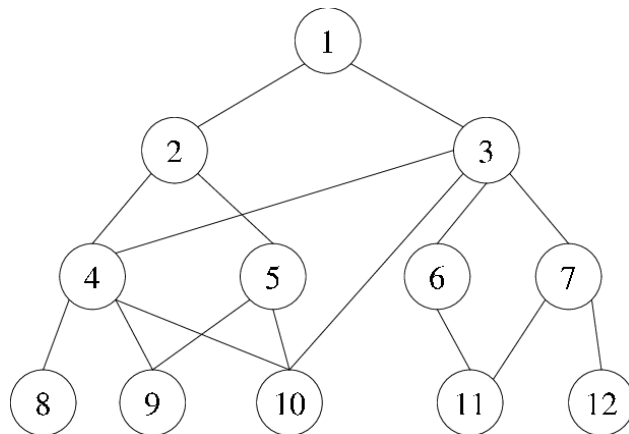


Figure 1.1: (Hasse Diagram) Because of transitivity, we can ignore the line between (1) and (5). Only the nearest neighbor relations are depicted, and the rest can be deduced from transitivity.

Local finiteness as described by Sorkin is “ a formal way of saying that a causal set is discrete.” The condition states that all order intervals in the set have finite cardinality. Cardinality

is the measure of the set's size or the number of elements in the set.

As suggested by Sumati Surya in her paper titled “Causal set approach to quantum gravity”, the essence of the HKMM theorem can be summarised as

$$\begin{aligned} \text{Causal Structure} + \text{Volume Element} &= \text{Lorentzian Geometry or,} \\ \text{Order} + \text{Number} &\sim \text{Lorentzian Geometry} \end{aligned}$$

This is called the “CST slogan” and ensures that an entire continuum spacetime geometry can be recovered from volume elements and causal order between events.

1.3.2 Continuum Approximation

The fundamental assumption of CST is that continuum spacetime can be approximated by discrete causal sets that have a volume element and causal relations. The question arises whether any causal set can approximate continuum spacetime.

To answer this question, we must first formalize what is meant by approximation. We almost define it as a mapping between a discrete causal set and continuum spacetime that is injective and structure-preserving (preserves global topological properties), called an Embedding. However, we also impose an extra condition, which requires the elements that are mapped to be uniformly distributed, and we call this a Faithful Embedding. Therefore, not all causal sets can approximate continuum spacetime arbitrarily; it must be faithfully embeddable. We call the causal sets that can be faithfully embedded as “**Manifold-like Causal Sets**”. In statistical terms, it is not feasible to create manifold-like causal sets starting from a poset with causal ordering because distinguishing between manifold-like and non-manifoldlike causal sets just by examining the causal set remains an unresolved issue. The majority of causal sets are typically found to be non-manifoldlike. Among the non-manifoldlike causal sets, a significant proportion are of the three-layer Kleitman-Rothschild (KR) type, which are illustrated in Fig. (1.2).

As discussed in Ref.², the process of generating manifold-like causal sets can be achieved by starting with a continuum spacetime or Lorentzian manifold. From this manifold, a countable number of elements are chosen to create the causal set. This process is called **Sprinkling**. A

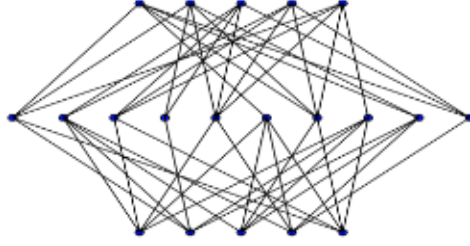


Figure 1.2: KR causal sets with 20 elements. As the number of elements increases, the ratio of KR causal sets to the total generated causal set approaches one.

primitive method of sprinkling involves placing the points on a regular grid, which appears to be evenly spaced. However, under a Lorentz boost, the spacing becomes distorted, leading to an uneven distribution. Therefore, a more sophisticated method is necessary to ensure that the resulting causal set is Lorentz invariant. To ensure Lorentz invariance, one method is to sprinkle points according to Poisson's distribution with an average density ρ_c . By using the Poisson distribution, the sprinkled points are distributed in a way that is invariant under Lorentz transformations, making it possible to generate manifold-like causal sets. The probability of finding n elements in a region of volume V through a Poisson distribution is given by

$$P_V(n) = \frac{(\rho_c V)^n}{n!} \exp(-\rho_c V), \quad (1.4)$$

where

$$\langle n \rangle = \rho_c V$$

We can also say that a Lorentzian manifold is said to be a continuum approximation to a causal set C if C can be obtained from a Poisson sprinkling in that manifold.

The Poisson process distribution allows for the concept of equivalence classes, which means that several causal sets can be approximated by a single Lorentzian manifold. These causal sets can be grouped together into the same class if they are generated from the same continuum spacetime. However, it is not possible for a single causal set to represent multiple continuum spacetimes. This is due to the **Hauptvermutung of CST**, a fundamental conjecture that states the following:

“A causal set can only be faithfully embedded into two spacetimes at the same density ρ_c if those spacetimes would be approximately isometric.”

This means that every causal set has a unique physical emergent spacetime continuum. If it were to approximate many continuum spacetimes, these spacetimes are identical at larger scales. However, they can differ at the Planckian scale.

Some of the Manifoldlike causal sets sprinkled using Poisson’s distribution are given below.

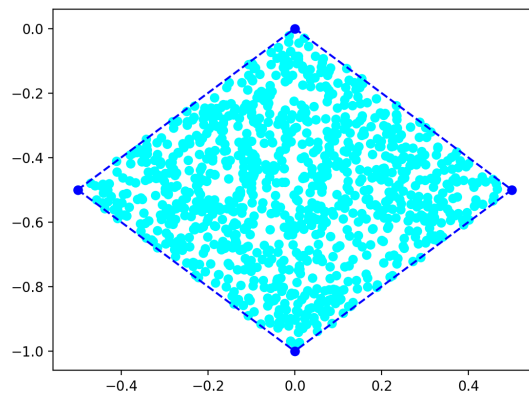


Figure 1.3: Manifoldlike Causal sets sprinkled in two-dimensional Minkowski Spacetime with total number of elements $N= 1000$

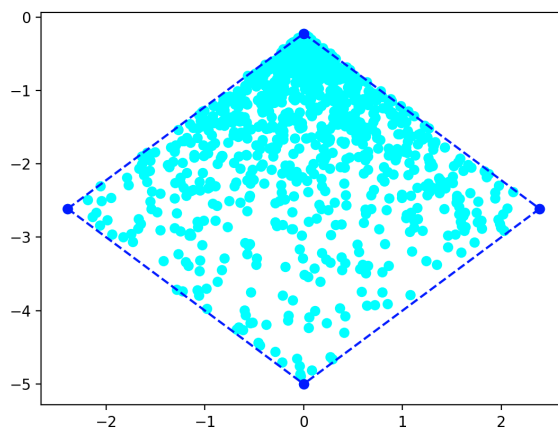


Figure 1.4: Manifoldlike Causal sets sprinkled in two-dimensional de Sitter Spacetime with total number of elements $N= 1000$

A detailed mechanics of generating these manifold-like causal sets can be found in Appendix (A).

CHAPTER 2

BENINCASA-DOWKER ACTION FOR CAUSAL SET

2.1 Non-Locality in CST and Quasi-local operator

In this chapter, we are trying to find a causal set analogue of the continuum action given by the Einstein-Hilbert action.

$$S_{EH} = \int \sqrt{-g} R(x) d^d x, \quad (2.1)$$

where, $c = 16\pi G = 1$, $g = |g_{\mu\nu}|$ and $R(x)$ is the scalar curvature of the spacetime.

As discussed in Ref.⁴, the causal set version of this action would be,

$$S_{CST} = l^d \sum_i R_i, \quad (2.2)$$

where, R_i is the scalar curvature at each element, and l is a length scale equal to $l = \rho^{-1/d}$.

The equations above show that in order to proceed, we must determine the equivalent of the scalar curvature in causal set theory. It's worth noting that scalar curvature is defined locally in spacetime. However, is a local region well-defined in discrete causal set theory? The answer is discussed in the paper by Sorkin Ref.⁵ as follow.

Consider an event located at the origin. Let u and v be null geodesics through the origin. Let a point in causal set 'a' be the nearest neighbor to the origin. The red line in the Fig. (2.1) represents the hyperbola that passes through 'a' and is defined as a set of all possible points that can be Lorentz transformed to 'a'. All points on this hyperbola are equidistant from the origin at a distance of one Planck length. Thus, any arbitrary point 'b' on the hyperbola also has the same distance from the origin as 'a'. We can create two Alexandrov intervals [defined in Sec (1.3.1)] between the origin and 'a' and 'b' respectively. Based on the current definitions of causal set

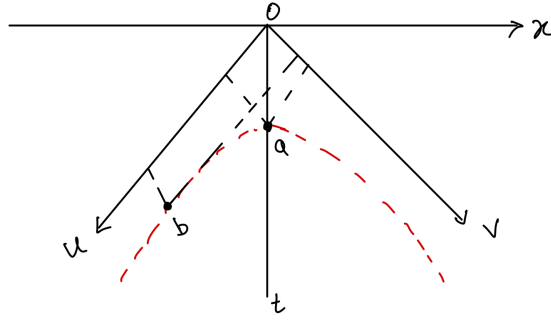


Figure 2.1: In CST, it is not possible to distinguish between local regions using either length or volume, even if one point (such as point a) is located in a local region with respect to the origin, while another point (such as point b) is not.

properties (link, chain, volume), can we determine which interval can be considered a local region in causal set theory? They both are at same distance ($l_a = l_b = \text{Planck length}$) and have no elements in between ($V_a = V_b = 0$), therefore, we cannot differentiate between these two intervals based on the fundamental properties of CST. So, the answer is “No”. Therefore, causal set theory is said to be fundamentally non-local. Non-locality is the price we must pay for working on a theory that is both discrete and Lorentz invariant.

Rafael Sorkin proposed a solution to the non-locality problem in CST by introducing a quasi-local scalar wave operator called $B^{(2)}$ for scalar fields on causal sets approximated by a two-dimensional Minkowski spacetime. The goal of this operator was to define local regions in the causal set. Sorkin showed that in the continuum limit, the operator tends to converge towards the two-dimensional flat scalar d’Alembertian, which is a locally defined operator. Benincasa extended this idea to four-dimensional spacetime by introducing an analogous operator called $B^{(4)}$ ⁶.

To express these operator as defined, we need to introduce the concept of layers in causal set.

A layer in a causal set refers to a subset of the causet, which is obtained by grouping the events having the same chain length with respect to a specific root element. For instance in

Fig. (2.2), Layer 1 is comprised of all the events that are located at one chain length from x . We can also define layers in terms of intervals. Layer one (L_1) is defined as the set of all Alexandrov intervals between an event (y) and x that have zero cardinality. To be more precise, if x is an event in a causet C , then we can define the set of all past neighborhood events of x that belong to the i th layer as follows:

$$L_i(x) = \{y \in C \mid y < x, n(x, y) = i - 1\}, \quad (2.3)$$

where $n(x, y)$ is the cardinality of the interval excluding end points.

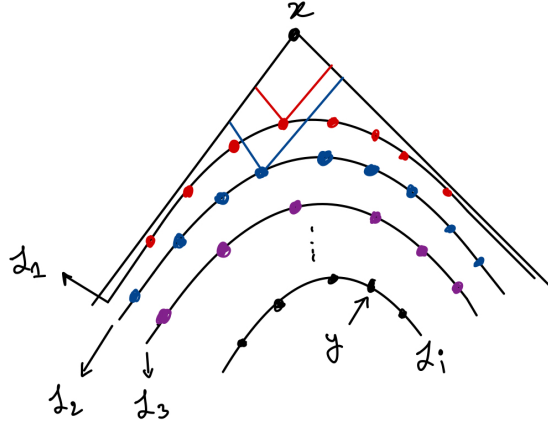


Figure 2.2: This Figure shows the concept of causal set layers, where the elements on the first hyperbolic line are equidistant from the origin and are therefore referred to as layer 1. In addition, the intervals for these elements have zero cardinality. This concept has been extended to higher layers as well.

For a scalar field with compact support defined as, $\phi : C \rightarrow \mathbb{R}$, Sorkin defined $B^{(2)}$ such that,

$$B^{(2)}\phi(x) = \frac{2}{l_p^0} \left[-\phi(x) + \left(2 \sum_{y \in L_1} -4 \sum_{y \in L_2} + 2 \sum_{y \in L_3} \right) \phi(y) \right] \quad (2.4)$$

Benincasa defined $B^{(4)}$ such that,

$$B^{(4)}\phi(x) = \frac{4}{\sqrt{6}l_p^2} \left[-\phi(x) + \left(\sum_{y \in L_1} -9 \sum_{y \in L_2} + 16 \sum_{y \in L_3} - 8 \sum_{y \in L_4} \right) \phi(y) \right] \quad (2.5)$$

Here, l is the length scale, and $\sum_{y \in L_i}$ is the total number of events in i th layer.

In the following section, we will explore how Benincasa employed this operator to define scalar curvature and action for the causal set.

2.2 Action using the Benincasa-Dowker method

In the previous section, it was discussed that Sorkin proved the operator $B^{(2)}$ could produce a two-dimensional flat scalar d'Alembertian under the continuum limit. The formal expression is shown as follows:

$$\lim_{\rho \rightarrow \infty} \langle B\phi(x) \rangle = \square\phi(x) \quad (2.6)$$

Benincasa extended this result not only to four-dimensional Minkowski spacetime but also to curved spacetime, given by:

$$\lim_{\rho \rightarrow \infty} \langle B\phi(x) \rangle = \square\phi(x) - \frac{1}{2}R(x) \quad (2.7)$$

A proof of Eq. (2.6) for four dimensions using the operator defined in Eq. (2.5) was proposed by Benincasa.⁶ The left-hand side (LHS) of Eq. (2.6) can be expressed as:

$$\lim_{\rho \rightarrow \infty} \langle B\phi(x) \rangle = \lim_{\rho \rightarrow \infty} \frac{4}{\sqrt{6}l_p^2} \left[-\langle \phi(x) \rangle + \langle \sum_{y \in L_1} \phi(y) \rangle - 9\langle \sum_{y \in L_2} \phi(y) \rangle + 16\langle \sum_{y \in L_3} \phi(y) \rangle - 8\langle \sum_{y \in L_4} \phi(y) \rangle \right] \quad (2.8)$$

In the context of a causal scalar field $\phi(x)$, the goal is to determine the expected value of the total number of elements in Layer 1, 2, 3, and 4. In order to accomplish this, the sprinkled spacetime is divided into small cells with volumes labelled by ' i ' and denoted as ΔV_i . For a given cell, let m_i be the total number of elements between the root element ' x ' and the i th cell. Additionally, each volume cell contains an average of $n_i = \sum_i \langle \chi_i \rangle$ sprinkled points, where χ_i is defined as,

$$\chi_i = \begin{cases} 1 & \text{if } i \text{ is filled} \\ 0 & \text{otherwise} \end{cases} \quad (2.9)$$

If we assume that the density of the causal set is uniform as $\rho = n_i/\Delta V$, where n_i is the

total number of elements in the i th cell of volume ΔV , then we can say $n_i = \sum_i \langle \chi_i \rangle = \rho \Delta V$. The main objective is to calculate the expected value of the total number of elements in different layers, starting with layer 1. We need to determine the probability of finding an element in layer 1, which is equivalent to finding the probability that the interval between the root element x and its past neighbor y has zero cardinality, i.e., $n(x, y) = 0$. The causal set is generated using Poisson's distribution, which implies that $\mu = \rho V_i$, where V_i is the volume between x and the i th cell.

$$P(m_i = 0) = \frac{(\rho V_i)^0}{0!} e^{-\rho V_i} = e^{-\rho V_i}. \quad (2.10)$$

Now, if $n_{L_1} = \sum_{y \in L_1}$ as a number of elements in layer 1,

$$\langle n_{L_1} \rangle = \sum_{y \in L_1} P(m_i = 0) n_i = \sum_{y \in L_1} \rho \Delta V e^{-\rho V_i}. \quad (2.11)$$

Now, take the limit that ΔV goes to dV , then $\sum_{y \in L_1}$ goes to $\int_{y \in J^-}$ and $V_i = V(x, y)$

Replacing $\xi = \rho V(x, y)$, we get

$$\langle n_{L_1} \phi(y) \rangle = \int_{y \in J^-} \rho dV e^{-\xi} \phi(y). \quad (2.12)$$

For Layer 2,

$$P(m_i = 1) = \frac{(\rho V_i)^1}{1!} e^{-\rho V_i} = \rho V_i e^{-\rho V_i}. \quad (2.13)$$

Then,

$$\langle n_{L_2} \rangle = \sum_{y \in L_2} P(m_i = 1) n_i = \sum_{y \in L_1} \rho^2 \Delta V V_i e^{-\rho V_i}. \quad (2.14)$$

Taking the limit yields

$$\langle n_{L_2} \phi(y) \rangle = \int_{y \in J^-} \rho \xi dV e^{-\xi} \phi(y). \quad (2.15)$$

Similarly,

$$\langle n_{L_3} \phi(y) \rangle = \int_{y \in J^-} \rho \frac{\xi^2}{2} dV e^{-\xi} \phi(y). \quad (2.16)$$

$$\langle n_{L_4} \phi(y) \rangle = \int_{y \in J^-} \rho \frac{\xi^3}{6} dV e^{-\xi} \phi(y). \quad (2.17)$$

Plugging these values into Eq. (2.8) and using $\rho = l^{-d}$, where d is the dimension,

$$\lim_{\rho \rightarrow \infty} \langle B\phi(x) \rangle = \lim_{\rho \rightarrow \infty} \frac{4\sqrt{\rho}}{\sqrt{6}} \left[-\phi(x) + \rho \int_{y \in J^-} dV \phi(y) e^{-\xi} \left(1 - 9\xi + 8\xi^2 - \frac{4}{3}\xi^3 \right) \right] \quad (2.18)$$

To evaluate the integration on the right-hand side (RHS) of Eq. (2.18), we need to establish a coordinate system. We can select the point x as the origin of a Cartesian coordinate system with coordinates y^μ , where the spatial polar coordinates are defined as $r = \sqrt{\sum_{i=1}^3 (y^i)^2}$, θ , and ϕ . We can also define null coordinates that point towards the past as $u = \frac{1}{\sqrt{2}}(-t - r)$ and $v = \frac{1}{\sqrt{2}}(-t + r)$. The volume $V(y)$ between the origin and point y is given by $V(y) = \frac{\pi}{6} u^2 v^2$. Let W be the integration region such that $u^2 + v^2 \leq L^2$, divided into three regions, W_1 , W_2 , and W_3 . W_1 is a neighborhood of the origin, W_2 is a neighborhood of the past light cone and is bounded away from the origin, and W_3 is a subset of the interior of the causal set that is bounded away from the origin and the boundary. This is illustrated in the figure below.

The regions as given in Fig. (2.3) are divided such that,

$$\begin{aligned} W_1 &= \{y \in W \mid 0 \leq u \leq v \leq a\}, \\ W_2 &= \{y \in W \mid a \leq v \leq L, 0 \leq u \leq \frac{a^2}{v}\}, \\ W_3 &= W / (W_1 \cup W_2), \end{aligned} \quad (2.19)$$

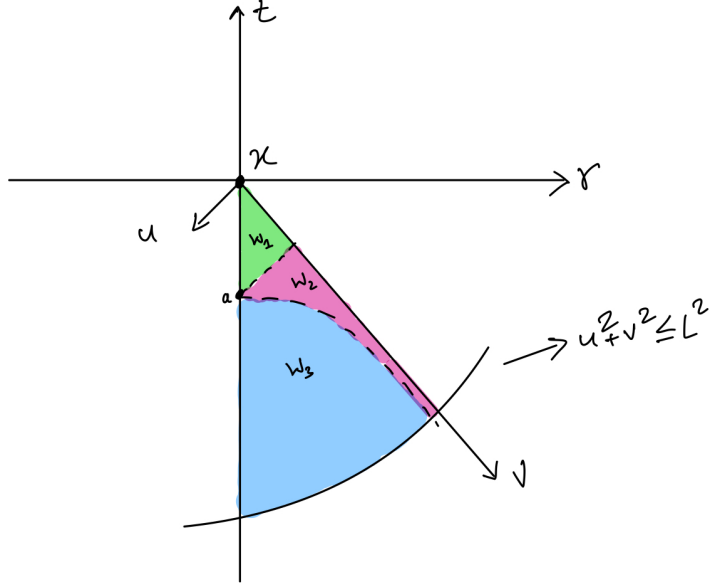


Figure 2.3: Partition of W into regions W_1 (Green), W_2 (Pink), W_3 (Blue) in $t - r$ plane. $a > 0$ is small enough that expansions of ϕ are valid.

Given that, $dV = \sqrt{-g} d^4y$, Eq. (2.18) looks like as follows,

$$\begin{aligned}
\lim_{\rho \rightarrow \infty} \langle B\phi(x) \rangle &= \lim_{\rho \rightarrow \infty} \frac{4\sqrt{\rho}}{\sqrt{6}} \left[-\phi(x) + \rho \int_{y \in W} \sqrt{-g} d^4y \phi(y) e^{-\xi} (1 - 9\xi + 8\xi^2 - \frac{4}{3}\xi^3) \right] \\
&= \lim_{\rho \rightarrow \infty} \frac{4\sqrt{\rho}}{\sqrt{6}} \left[-\phi(x) + \rho \left(\int_{y \in W_1} \sqrt{-g} d^4y \phi(y) e^{-\xi} (1 - 9\xi + 8\xi^2 - \frac{4}{3}\xi^3) \right. \right. \\
&\quad + \int_{y \in W_2} \sqrt{-g} d^4y \phi(y) e^{-\xi} (1 - 9\xi + 8\xi^2 - \frac{4}{3}\xi^3) \\
&\quad \left. \left. + \int_{y \in W_3} \sqrt{-g} d^4y \phi(y) e^{-\xi} (1 - 9\xi + 8\xi^2 - \frac{4}{3}\xi^3) \right) \right] \tag{2.20}
\end{aligned}$$

Benincasa's findings suggest that as the density ρ approaches infinity, the value of the integral within regions W_2 and W_3 will become negligible, leaving the only significant contribution coming from W_1 , which is the neighborhood of the origin. This ultimately leads to $\lim_{\rho \rightarrow \infty} \langle B\phi(x) \rangle$ being equivalent to the continuum d'Alembertian in Minkowski spacetime, i.e. $g_{\mu\nu} = \eta_{\mu\nu}$ and $\sqrt{-g} = 1$, where $g = \det g_{\mu\nu}$ as shown in Eq. (2.6).

In order to connect this expression to the action, we need to investigate its behavior in curved spacetime. To achieve generality, we can expand the metric using Riemann normal coordinates in

Eq. (2.20), with an approximation up to first order, where R can be any component of the Riemann tensor, Ricci tensor, or scalar curvature. The Riemann Normal Coordinate (RNC) system describes a point x_0 within a spacetime by using a convex normal neighborhood Q . This neighborhood Q is a subset of M where the exponential map $\exp: T_p M \rightarrow Q$ is a diffeomorphism for any point p within Q . In the RNC system, the coordinates of Q are determined by the geodesics originating from x_0 , and the metric at x_0 is considered to be flat, meaning that $g_{\mu\nu}(x_0) = \eta_{\mu\nu}$ and $\left. \frac{\partial}{\partial g_{\mu\nu}} \right|_{x_0} = 0$. Consequently, the Christoffel connection is zero, allowing the metric at any point x within Q to be expanded as follows.⁷

$$g_{\mu\nu} = \eta_{\mu\nu} - \frac{1}{3}(x - x_0)^\alpha (x - x_0)^\beta R_{\mu\alpha\nu\beta}(x_0) \quad (2.21)$$

For small variable ϵ , $\det(I + \epsilon X)$ can be expressed as $\det(I) + \text{tr}(X)\epsilon + O(\epsilon^2)$, where $\text{tr}(X)$ denotes the trace of the matrix X . The term $O(\epsilon^2)$ indicates higher-order terms of ϵ that are negligible in the approximation.

As such the determinant of the metric in Eq. (2.21) will be given by,

$$g = \det(g_{\mu\nu}) = -1 + \frac{1}{3}(x - x_0)^\alpha (x - x_0)^\beta R_{\alpha\beta}(x_0) \quad (2.22)$$

Thus,

$$\sqrt{-g} = 1 - \frac{1}{6}(x - x_0)^\alpha (x - x_0)^\beta R_{\alpha\beta}(x_0) \quad (2.23)$$

Imposing this condition in Eq. (2.20) leads to,

$$\lim_{\rho \rightarrow \infty} \langle B\phi(x) \rangle = \square\phi(x) - \frac{1}{2}R(x) \quad (2.24)$$

In the present scenario, considering a scalar field in two dimensions defined by a constant,

$\phi : C \rightarrow -2$, and inverting Eq. (2.24) provides us with the following expression:

$$\begin{aligned}
R(x) &= \lim_{\rho \rightarrow \infty} \langle B^{(2)}(-2) \rangle - \square(-2) \\
&= \lim_{\rho \rightarrow \infty} \left\langle \frac{2}{l^0_p} \left(2 + \left(2 \sum_{y \in L_1(x)} -4 \sum_{y \in L_2(x)} + 2 \sum_{y \in L_3(x)} \right) (-2) \right) \right\rangle \\
&= \lim_{\rho \rightarrow \infty} \left\langle 4 \left(1 - 2 \sum_{y \in L_1(x)} + 4 \sum_{y \in L_2(x)} - 2 \sum_{y \in L_3(x)} \right) \right\rangle
\end{aligned} \tag{2.25}$$

As stated in Surya's paper,² we can write the dimensionless discrete Ricci curvature at an element $i \in C$ as,

$$R_i = 4(1 - 2N_1(i) + 4N_2(i) - 2N_3(i)) \tag{2.26}$$

Here, the $N_k(i)$ represent the order intervals in the causal set which contain $i + 1$ elements including the end points. Summing over the N elements of a finite element causal set gives the discrete action as,

$$\begin{aligned}
S &= l^2 \sum_{i \in C} R_i \\
&= 4l^2 \sum_{i \in C} (1 - 2N_1(i) + 4N_2(i) - 2N_3(i)), \\
&= 4(N - 2N_1 + 4N_2 - 2N_3)
\end{aligned} \tag{2.27}$$

In this context, $l = 1$ and the variable N refers to the total number of elements in the causal set C . N_i refers to the total number of $i + 1$ element order intervals (including end points) in C .

In the case of Minkowski spacetime, we anticipate that the action will become zero as N approaches large value since the curvature is zero. In contrast, in de Sitter spacetime, the action should be equivalent to $(2H^2 \cdot V)$ in continuum, where H is the hubble parameter.

Figures (2.4)–(2.5) illustrate the considerable uncertainty in the average value of BD action across 50 different causal sets simulations, with error bars spanning several orders of magnitude,

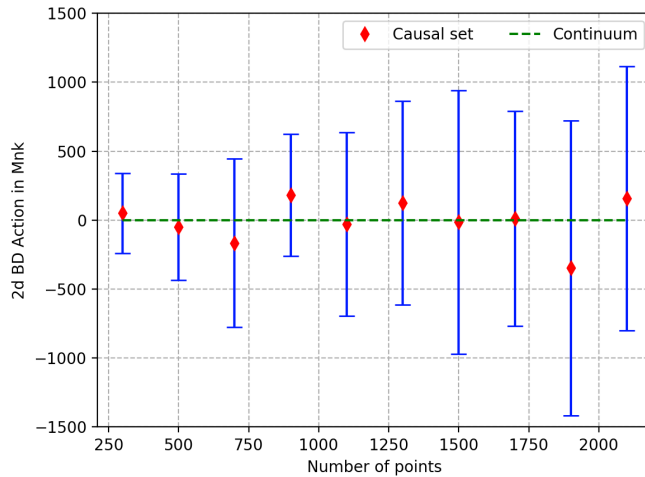


Figure 2.4: The graph shows the Benincasa-Dowker action plotted against the number of randomly sprinkled points in Minkowski spacetime. This graph is the result of averaging 50 different causal sets for each value of N . As the number of points N increases, it appears that the fluctuations in the graph also increase.

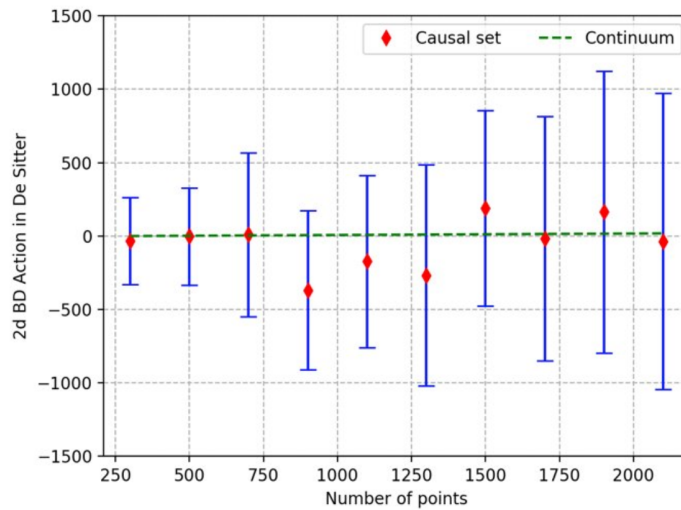


Figure 2.5: The graph shows the Benincasa-Dowker action plotted against the number of randomly sprinkled points in de Sitter spacetime with Hubble parameter equal to 100. This graph is the result of averaging 50 different causal sets for each value of N . As the number of points N increases, it appears that the fluctuations in the graph also increase.

from 10^2 to 10^3 . Notably, as the number of points increases, the magnitude of these error bars also grows. This trend can be attributed to the terms in Eq. (2.27) that arise directly from Poisson's distribution, which inherently leads to increased uncertainty with a larger number of points. Another

possible error could come from the fact that the result was obtained by neglecting all terms beyond the linear term in the Riemann tensor's metric expansion. As more points are added, the higher-order terms become more significant and cannot be ignored. Despite some advantages of using BD to calculate action, the large error bars must not be overlooked. Another efficient approach to calculating action, known as "Chain Action," proposed by Dr. Luca Bombelli and Dr. B. B. Pilgrim,⁴ will be discussed in the next chapter.

CHAPTER 3

CHAIN ACTION FOR CAUSAL SET

A chain in a causal set between two points, a_0 and a_k , of length k is a sequence of $k + 1$ related points arranged in a specific order, $a_0 < a_1 < a_2 \dots < a_k$. The total number of k -chains depend on the distribution of the points within the interval. The accompanying figure provides a clearer explanation of this concept.

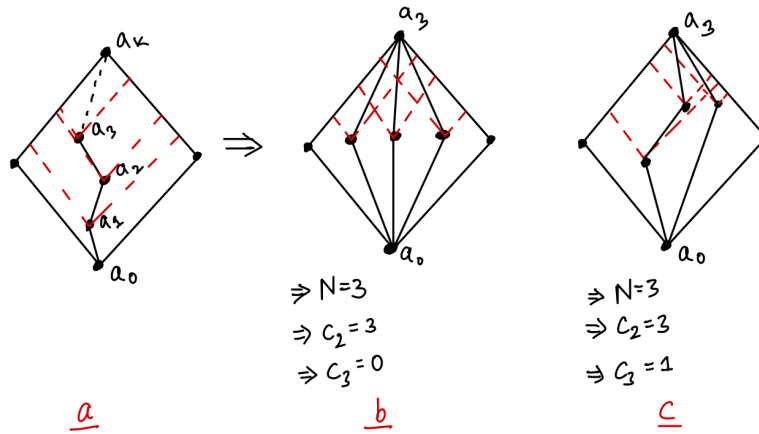


Figure 3.1: a) An Alexandrov set displays the sequence of $a_0 < a_1 < a_2 \dots < a_k$ with the minimum point being a_0 and the maximum point being a_k . The red dot line denotes the null rays from the point. (b) One example of distributing three elements within the interval such that $C_3 = 0$ (c) Another example of distributing three elements in the same interval such that $C_3 = 1$.

As shown in Fig. (3.1)(b) and (c), the number of 3-chains in a causal set appears to be influenced by how the points are distributed within the interval. The distribution of points in the causal set determines the distribution of chain lengths. On the other hand, if we examine Fig. (1.3)-(1.4) from the first chapter, we can see a significant difference in the distribution of points within

the interval for Minkowski spacetime (no curvature) and de Sitter spacetime (positive curvature). This highlights an important correlation between chain length distribution and the curvature of spacetime. The simulation for the distribution of k -chain abundance affected by the choice of spacetime for same number of points $N = 500$ is given in Fig. (3.2).

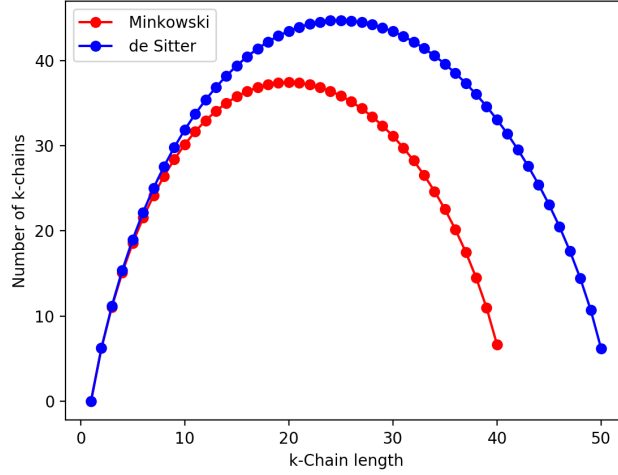


Figure 3.2: Distribution of k -chain abundance as a function of k -chain length for Minkowski and de Sitter spacetime.

In the next section, we will take advantage of this relationship to determine the scalar curvature and eventually the action.

3.1 Chain Length Distribution

The binomial distribution provides the probability of finding precisely k points within a volume V of N uniformly distributed points in a larger volume V_0 ,

$$P_k = \binom{N}{k} \left(\frac{V}{V_0}\right)^k \left(1 - \frac{V}{V_0}\right)^{N-k} \quad (3.1)$$

If V_0 is much larger than V , we can use Poisson's distribution of density $\rho = N/V_0$ to estimate the probability density. Therefore, the likelihood of having one point in a very small volume element dV can be expressed as $\rho dV = (N/V_0)dV$. As illustrated in the paper by Aghili⁸, the probability of having one point in each of the $k - 1$ differential volumes can be determined in a

similar way.

$$\rho_0 dV_1 \rho_1 dV_2 \dots \rho_{k-2} dV_{k-1} + \text{H.O.T.}, \quad (3.2)$$

where $\rho_i = (N - i)/V_0$.

Dr. Pilgrim discusses in his paper⁴ states that this probability density considers the points that have already been placed. For example, $\rho_1 dV_2 = \frac{N-1}{V_0} dV_2$ represents the probability of finding one point in an infinitesimal volume dV_2 if there is already one point in dV_1 . For an Alexandrov set A_0 with a minimum point a_0 and a maximum point a_k , Eq. (3.2) gives the probability of a chain of length k existing between a_0 and a_k through the differential volumes $dV_1, dV_2, \dots, dV_{k-1}$.

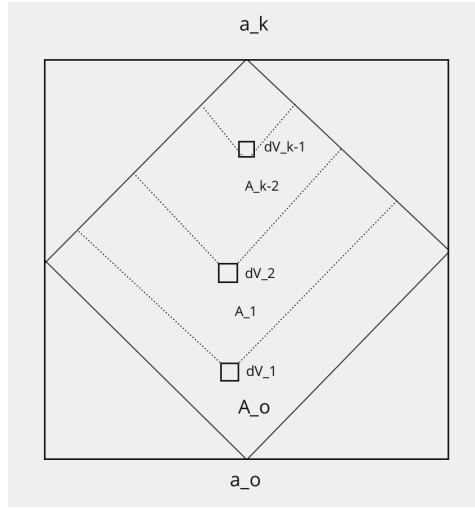


Figure 3.3: A graphical depiction of how chains are acquired.

Once we have the probability distribution function, it is a straightforward integration of the probability from Eq. (3.2) over the Alexandrov interval A_i , where $dV_i \in A_{i-1}$, to calculate the mean number of chain length k between minimal and maximal point. Given that $dV_i = \sqrt{-g_i} d^d y_i$,

$$\langle C_k \rangle = \rho_0 \int_{A_0} \sqrt{-g_1} d^d y_1 \cdot \rho_1 \int_{A_1} \sqrt{-g_2} d^d y_2 \cdot \rho_2 \int_{A_2} \sqrt{-g_3} d^d y_3 \dots \rho_{k-2} \int_{A_{k-2}} \sqrt{-g_{k-1}} d^d y_{k-1} \quad (3.3)$$

3.2 Chain length distribution in Minkowski spacetime

Let's look at this in 2-dimensions Minkowski spacetime with null coordinates (u, v) which are defined as follows, $x = (u - v)/\sqrt{2}, t = (u + v)/\sqrt{2}$. The volume of an Alexandrov interval

between (u_0, v_0) and (u_k, v_k) using $dV = \sqrt{-g} du_k dv_k$ is given by,

$$\begin{aligned}
 V &= \int_A \sqrt{-g} du_k dv_k \\
 &= \int_{u_0}^{u_k} du_k \int_{v_0}^{v_k} dv_k \\
 &= (u_k - u_0)(v_k - v_0)
 \end{aligned}
 \tag{3.4}$$

Here, $\sqrt{-g} = 1$. Let's start with the simple nontrivial cases of chain length distributions, $\langle C_3 \rangle$, $\langle C_4 \rangle$, as illustrated in the figure below.

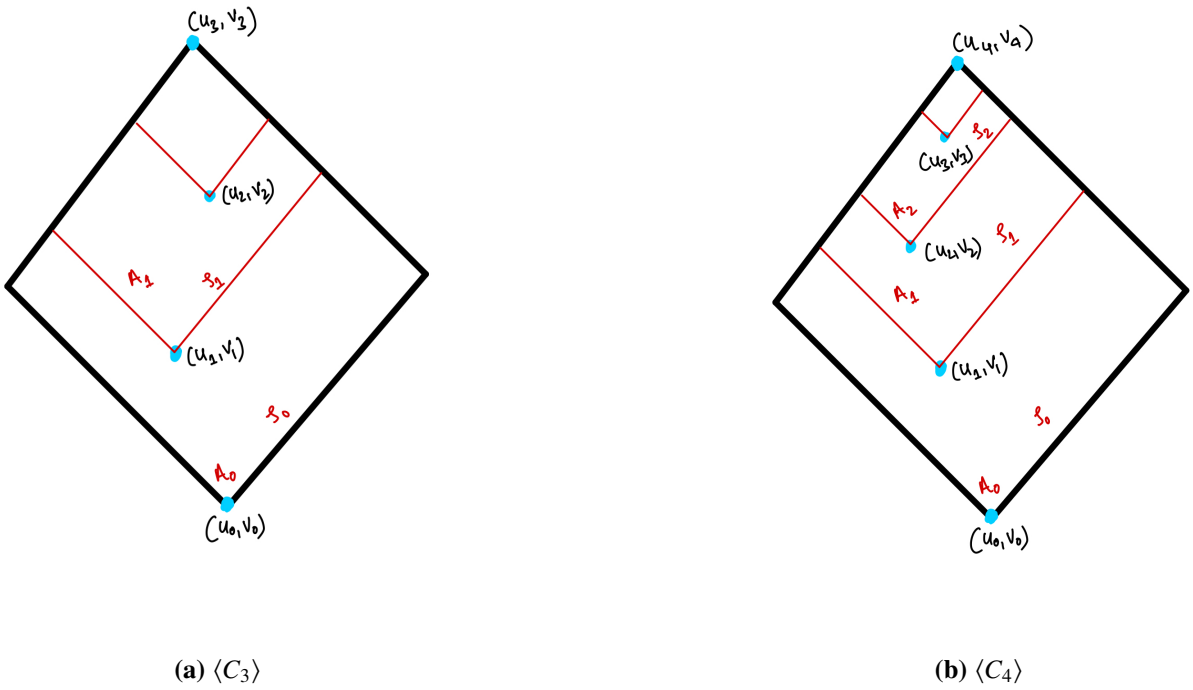


Figure 3.4: Visual representation of region of integration for $\langle C_3 \rangle$ and $\langle C_4 \rangle$.

Integrating eq 3.3 keeping in mind that $\rho_i = \frac{N-i}{V}$, $V^2 = (u_3 - u_0)^2(v_3 - v_0)^2$, we get

$$\begin{aligned}
\langle C_3 \rangle &= \rho_0 \int_{A_0} du_1 dv_1 \cdot \rho_1 \int_{A_1} du_2 dv_2 \\
&= \frac{N(N-1)}{V^2} \left(\int_{u_0}^{u_3} du_1 \int_{v_0}^{v_3} dv_1 \cdot \int_{u_1}^{u_3} du_2 \int_{v_1}^{v_3} dv_2 \right) \\
&= \frac{N(N-1)}{V^2} \left(\frac{(u_3 - u_0)^2 (v_3 - v_0)^2}{4} \right) \\
&= \frac{N!}{4(N-2)!}
\end{aligned} \tag{3.5}$$

Similarly for $k = 4$, we have

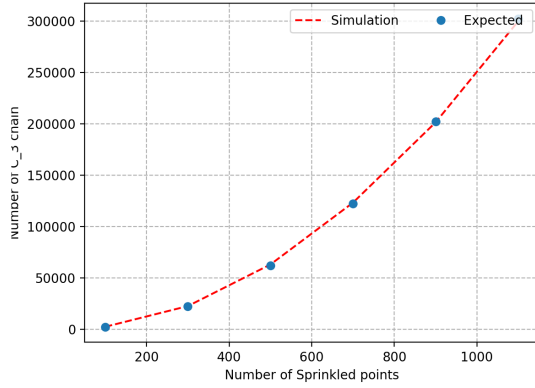
$$\begin{aligned}
\langle C_4 \rangle &= \rho_0 \int_{A_0} du_1 dv_1 \cdot \rho_1 \int_{A_1} du_2 dv_2 \cdot \rho_2 \int_{A_2} du_3 dv_3 \\
&= \frac{N(N-1)(N-2)}{V^3} \left(\int_{u_0}^{u_4} du_1 \int_{v_0}^{v_4} dv_1 \cdot \int_{u_1}^{u_4} du_2 \int_{v_1}^{v_4} dv_2 \cdot \int_{u_2}^{u_4} du_3 \int_{v_2}^{v_4} dv_3 \right) \\
&= \frac{N(N-1)(N-2)}{V^3} \left(\frac{(u_3 - u_0)^3 (v_3 - v_0)^3}{36} \right) \\
&= \frac{N!}{36(N-3)!}
\end{aligned} \tag{3.6}$$

In a recent publication authored by Dr. Pilgrim and Dr. Bombelli⁴, they presented the generalized equation for the expected number of k -chains with a dimension of d as follows,

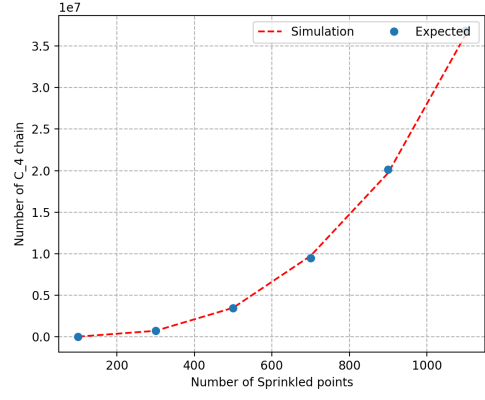
$$\langle C_k \rangle = \frac{N!}{(N-k+1)!} \left(\frac{\Gamma(d+1)}{2} \right)^{k-2} \frac{\Gamma(d/2+1)\Gamma(d)}{\Gamma((k-1)d/2+1)\Gamma(kd/2)} \tag{3.7}$$

The validity of this result can be confirmed through computer simulations involving the calculation of the number of 3-chains and 4-chains as demonstrated in Fig. (3.5).

Figure (3.5) shows the gathered simulated data for 3-chains and 4-chains by taking the average of 25 various causal sets. If we do not perform averaging, there is a possibility of some fluctuation in the final outcome. It is observed that the expected numbers of 3-chains and 4-chains utilizing Eq. (3.7) is highly accurate to the extent that it is almost equal to the simulated value. This verifies our formula for chain length distribution in a flat spacetime.



(a) $\langle C_3 \rangle$ vs N



(b) $\langle C_4 \rangle$ vs N

Figure 3.5: A graph comparing the expected number of chain length-3, 4 according to (3.7) with the simulation.

3.3 Chain length distribution in Curved spacetime

In our pursuit to establish the connection between chain distribution and curvature, extending the findings to curved spacetime seems to be a natural progression. Dr. Pilgrim, in his doctoral thesis,⁹ successfully derived this relationship in the context of 2-dimensional curved spacetime by expanding the metric using Riemann normal coordinates up to the linear term in R . The metric in the vicinity of (x_0, t_0) can be expressed through the following expansion:

$$g_{\mu\nu} = \eta_{\mu\nu} - \frac{1}{3}(x - x_0)^\alpha (x - x_0)^\beta R_{\mu\alpha\nu\beta}(x_0). \quad (3.8)$$

The line element in two dimension will take this form,

$$\begin{aligned} ds^2 &= g_{\mu\nu} dx^\mu dx^\nu \\ &= g_{00} dx^0 dx^0 + g_{11} dx^1 dx^1 + g_{01} dx^0 dx^1 + g_{10} dx^1 dx^0 \\ &= \left(-1 + \frac{R}{6}(x - x_0)^2\right) dt^2 + \left(1 + \frac{R}{6}(t - t_0)^2\right) dx^2 - \frac{R}{6}(x - x_0)(t - t_0)(dt dx + dx dt) \end{aligned} \quad (3.9)$$

In two-dimensional spacetime, the Riemann curvature tensor has only one independent component. This means that the curvature is completely determined by a single scalar quantity

known as the scalar curvature (denoted by R). Thus,

$$R = g^{\mu\nu} g^{\alpha\beta} R_{\alpha\mu\beta\nu} = \eta^{\mu\nu} \eta^{\alpha\beta} R_{\alpha\mu\beta\nu} = \eta^{\mu\nu} (R_{0\mu 0\nu} + R_{1\mu 1\nu}) = -R_{0101} - R_{1010} = -2R_{0101} \quad (3.10)$$

Here, we made the assumption that the product of two inverse metric tensors, namely $g^{\mu\nu} g^{\alpha\beta}$, is equal to $\eta^{\mu\nu} \eta^{\alpha\beta}$. It is because we are only interested in the linear terms in the scalar curvature. By using this expression for the Riemann curvature, values of g_{00} , g_{11} , g_{01} , and g_{10} were determined through Eq. (3.8), leading us to Eq. (3.9).

In two dimensions, it is always possible to find an appropriate coordinate transformation that will put the metric in conformally flat form. Conformally flat metrics have the advantage of allowing the use of coordinate systems resembling Cartesian coordinates, which simplifies calculations and transformations. When using this coordinate representation, we do not need to be concerned about the presence of boundary terms during integration. In two-dimensional curved spacetime, as states in the works of Dr. Pilgrim,⁹ the coordinate transformation takes the form below,

$$\begin{aligned} t &= \frac{u+v}{\sqrt{2}} + \frac{R}{12\sqrt{2}} ((v-v_0)(u-u_0)^2 + (v-v_0)^2(u-u_0)) \\ x &= \frac{u-v}{\sqrt{2}} + \frac{R}{12\sqrt{2}} ((v-v_0)(u-u_0)^2 - (v-v_0)^2(u-u_0)) \end{aligned} \quad (3.11)$$

To understand the process of obtaining this coordinate transformation, we start by taking the Minkowski null coordinates ($x = (u-v)/\sqrt{2}$, $t = (u+v)/\sqrt{2}$) and adding terms that are linear in the scalar curvature with the appropriate combination of $(v-v_0)$ and $(u-u_0)$ that preserves the dimensionality. This is given below,

$$\begin{aligned} t &= \frac{u+v}{\sqrt{2}} + R(C(v-v_0)(u-u_0)^2 + D(v-v_0)^2(u-u_0)) \\ x &= \frac{u-v}{\sqrt{2}} + R(A(v-v_0)(u-u_0)^2 + B(v-v_0)^2(u-u_0)) \end{aligned} \quad (3.12)$$

From these, we can derive the expressions for $(x^2, t^2, dx, dt, dx^2, dt^2, dxdt)$ in terms of the

null coordinates (u, v) . By directly substituting these expressions into Eq. (3.9), we obtain the line element of form as shown in Eq. (3.13). Throughout the calculations, we maintain the consideration of only the linear order of scalar curvature.

$$\begin{aligned}
ds^2 = & \text{Minkowski part} + \frac{R}{12}(2u^2 dv^2 - 4uv dudv + 2v^2 du^2) \\
& + R\sqrt{2}[A(2uv du^2 + u^2 dudv - 2uv dudv - u^2 dv^2) + B(2uv dudv + v^2 du^2 - 2uv dv^2 - v^2 dudv) \\
& + C(-2uv du^2 - u^2 dudv - 2uv dudv - u^2 dv^2) + D(-2uv dudv - v^2 du^2 - 2uv dv^2 - v^2 dudv)]
\end{aligned} \tag{3.13}$$

By choosing

$$A = \frac{1}{12\sqrt{2}}, B = -\frac{1}{12\sqrt{2}}, C = \frac{1}{12\sqrt{2}}, D = \frac{1}{12\sqrt{2}}$$

The line element can be reduced to,

$$ds^2 = -(2 + R(v - v_0)(u - u_0))dudv \tag{3.14}$$

We now want to investigate how the volume of an Alexandrov set A in curved spacetime with interval (u_0, v_0) and (u_k, v_k) has changed from Minkowski spacetime. The metric is expanded about (u_0, v_0) .

In this case,

$$\det(g_{\mu\nu}) = g(u_k, v_k) = -(1 + \frac{R}{2}(v_k - v_0)(u_k - u_0))^2 = -(1 + R(v_k - v_0)(u_k - u_0)) \tag{3.15}$$

thus,

$$\sqrt{-g(u_k, v_k)} = 1 + \frac{R}{2}(v_k - v_0)(u_k - u_0) \tag{3.16}$$

Now, the volume is given by

$$\begin{aligned}
V &= \int_A \sqrt{-g(u_k, v_k)} du_k dv_k \\
&= \int_{u_0}^{u_k} \int_{v_0}^{v_k} \left(1 + \frac{R}{2}(v_k - v_0)(u_k - u_0)\right) du_k dv_k \\
&= (u_k - u_0)(v_k - v_0) + \frac{R}{8}((v_k - v_0)^2(u_k - u_0)^2)
\end{aligned} \tag{3.17}$$

Using binomial expansion, we have

$$V^{k-1} = (u_k - u_0)^{k-1}(v_k - v_0)^{k-1} + \frac{R(k-1)}{8}(v_k - v_0)^k(u_k - u_0)^k \tag{3.18}$$

We are now ready to integrate Eq. (3.3) for 2-dimensional curved spacetime keeping only the linear term in the scalar curvature,

Let's start with $\langle C_3 \rangle$,

$$\begin{aligned}
\langle C_3 \rangle &= \rho_o \int_{A_0} \left(1 + \frac{R}{2}(v_3 - v_1)(u_3 - u_1)\right) du_1 dv_1 \cdot \rho_1 \int_{A_1} \left(1 + \frac{R}{2}(v_3 - v_2)(u_3 - u_2)\right) du_2 dv_2 \\
&= \frac{N(N-1)}{V^2} \left(\int_{u_0}^{u_3} du_1 \int_{v_0}^{v_3} dv_1 \left(1 + \frac{R}{2}(v_3 - v_1)(u_3 - u_1)\right) \right. \\
&\quad \cdot \left. \int_{u_1}^{u_3} du_2 \int_{v_1}^{v_3} dv_2 \left(1 + \frac{R}{2}(v_3 - v_2)(u_3 - u_2)\right) \right) \\
&= \frac{N!}{V^2(N-2)!} \left[\int_{A_0} du_1 dv_1 \cdot \int_{A_1} du_2 dv_2 + \frac{R}{2} \left(\int_{A_0} du_1 dv_1 \cdot \int_{A_1} du_2 dv_2 (v_3 - v_2)(u_3 - u_2) \right. \right. \\
&\quad \left. \left. + \int_{A_0} du_1 dv_1 (v_3 - v_1)(u_3 - u_1) \cdot \int_{A_1} du_2 dv_2 \right) \right] \\
&= \frac{N!}{V^2(N-2)!} \left[\frac{(u_3 - u_0)^2(v_3 - v_0)^2}{4} + \frac{5R}{72}(u_3 - u_0)^3(v_3 - v_0)^3 \right]
\end{aligned} \tag{3.19}$$

Let's subtract and add $\frac{R(u_3 - u_0)^3(v_3 - v_0)^3}{16}$ and use $V^2 = (u_3 - u_0)^2(v_3 - v_0)^2 + \frac{R}{4}(u_3 - u_0)^3(v_3 - v_0)^3$ to get

$$\langle C_3 \rangle = \frac{N!}{V^2(N-2)!} \left[\frac{V^2}{4} + \frac{R}{144}(u_3 - u_0)^3(v_3 - v_0)^3 \right] \tag{3.20}$$

Using $RV^3 = RV^2 \cdot \frac{N}{\rho} = R(u_3 - u_0)^3(v_3 - v_0)^3$ gives

$$\langle C_3 \rangle = \frac{N!}{(N-2)!} \left[\frac{1}{4} + \frac{1}{144} \frac{NR}{\rho} \right] \quad (3.21)$$

For k -chain, the generalized version of the expectation value of chain number⁹ is

$$\langle C_k \rangle = \frac{N!}{(N-(k-1))!} \left(\frac{1}{((k-1)!)^2} + \frac{NR}{\rho} \left(\frac{2k^3 - 3k^2 + k}{12(k!)^2} - \frac{k-1}{8((k-1)!)^2} \right) \right) \quad (3.22)$$

We would want to verify if this result holds true to causal sets created by sprinkling points in de Sitter spacetime with a scalar curvature of $R = 2H^2$, where H represents the Hubble parameter. Figure (3.6) illustrates that the calculated expected value of chain length 3, as determined by Eq. (3.22), aligns closely with the simulation results when considering a small number of points. However, as the number of points grows larger, the linear term of the scalar curvature becomes insufficient to capture the complete geometric information. Consequently, the accuracy begins to deviate from the simulation.

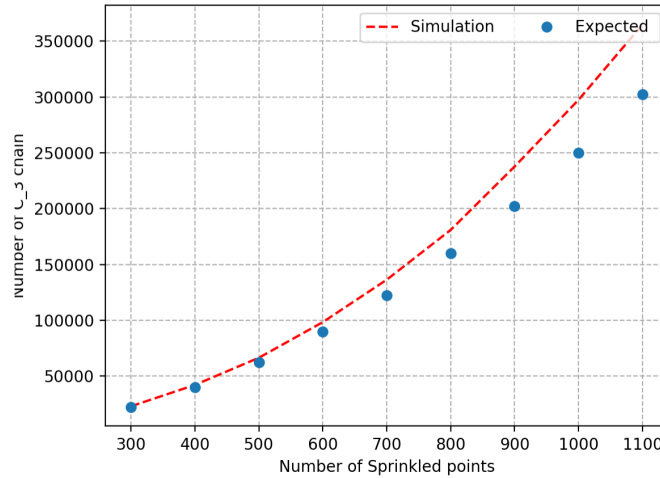


Figure 3.6: A graph comparing the Expected number of 3-chains using equation (3.22) and the actual average number of 3-chain obtained by sprinkling elements in a causal set of dimension 2 in de Sitter spacetime, plotted against the number of points in the causal set.

3.4 Chain Action

Eq (3.22) serves as the connection between chain length and scalar curvature which was mentioned at the beginning of this chapter. We can now invert this formula and calculate the scalar curvature in terms of k -chain length as follows.

$$R_k = \frac{\rho}{N} \cdot \left(\langle C_k \rangle \cdot \frac{(N-k+1)!}{N!} - \frac{1}{((k-1)!)^2} \right) \cdot \frac{1}{\left(\frac{2 \cdot k^3 - 3 \cdot k^2 + k}{12 \cdot (k!)^2} - \frac{k-1}{8 \cdot ((k-1)!)^2} \right)} \quad (3.23)$$

From our previous discussion, it is evident that the estimation of scalar curvature becomes less accurate as the number of points increases. However, it is still intriguing to observe the behavior of scalar curvature in relation to the chain length since scalar curvature is determined for each k .

In the regime where the significant contribution to the scalar curvature comes from its linear part, we can make the following claim in (2.2),

$$\text{For, } V = l^d = \frac{N}{\rho}, \quad S_{cst} = l^d \sum_i R_i \approx RV \quad (3.24)$$

Now plugging in (3.23) to (3.24), we get

$$S_k = \frac{N}{\rho} \cdot R_k = \left(\langle C_k \rangle \cdot \frac{(N-k+1)!}{N!} - \frac{1}{((k-1)!)^2} \right) \cdot \frac{1}{\left(\frac{2 \cdot k^3 - 3 \cdot k^2 + k}{12 \cdot (k!)^2} - \frac{k-1}{8 \cdot ((k-1)!)^2} \right)}. \quad (3.25)$$

Because of the definition of R in Eq. (3.23), instead of a single action, we now have a collection of actions associated with each value of k . It is intriguing to explore how the action can be computed for each k in various spacetime scenarios.

Figures (3.7)- (3.8) indicate that the error bars of the chain action are of order 1, and more importantly, they decrease as the number of points increases. In contrast to the BD action, which

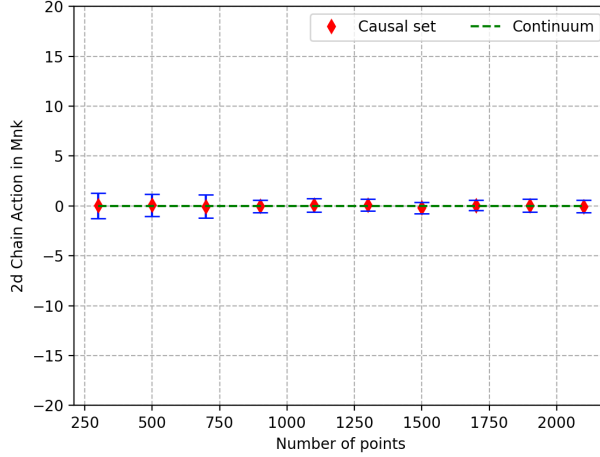
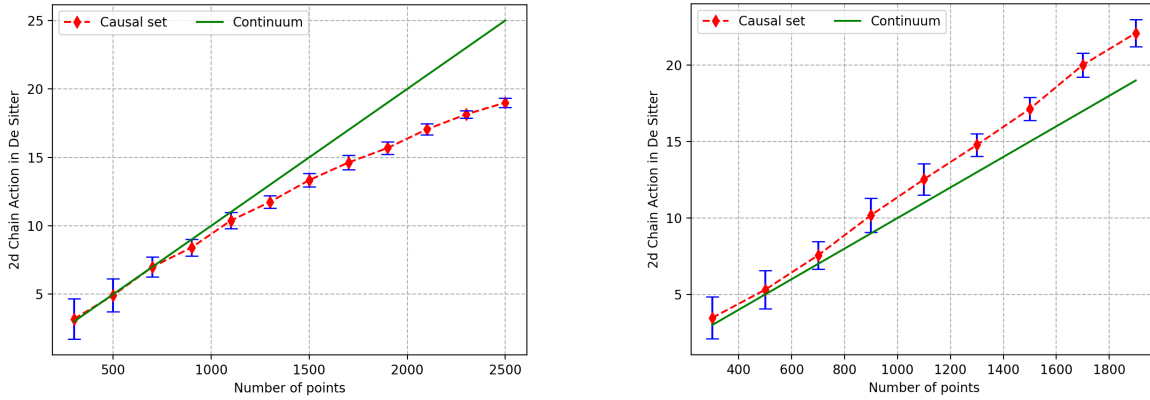


Figure 3.7: The graph shows the Chain action (S_3) for chain length 3 plotted against the number of randomly sprinkled points in Minkowski spacetime. This graph is the result of averaging 50 different causal sets for each N . As the number of points N increases, it appears that the fluctuations in the graph decrease and the action converge to continuum value.



(a) Chain action for de sitter spacetime for chain length 3 with $H = 100$ and $\rho = 2,000,000$ (b) Chain action for de sitter spacetime for chain length 4 with $H = 100$ and $\rho = 2,000,000$

Figure 3.8: This graph is the result of averaging 50 different causal sets. As the number of points N increases, it appears that the fluctuations in both of the graph decreases, however the average value deviates away from the continuum value.

was calculated in the previous section and had statistical fluctuations of order $10^2 - 10^3$, the chain action appears to have significantly less statistical fluctuation. However, one of the drawbacks of this approach is that for de Sitter spacetime as in Fig. (3.8), the action deviates from the continuum value as the number of points increases. This is due to the fact that only the linear terms of the

Scalar curvature are considered during the full derivation of chain action. If we include its higher order terms, the red dot in Fig. (3.8) for S_3 and S_4 should converge towards the continuum value (green line).

Figure (3.8) was generated with a curvature value of $H = 100$. If we were to reduce the curvature to $H = 50$, the action using linear approximation to scalar curvature would approach the value seen in the continuum as shown in Fig. (3.9) even for higher number of points. This suggests that the linear scalar curvature is able to capture most of the curvature in this regime.

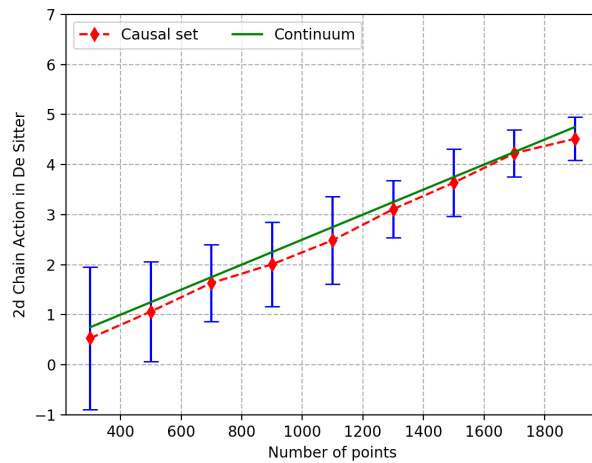


Figure 3.9: The graph illustrates the behavior of Chain action in de Sitter spacetime for $H = 50$ and $\rho = 2,000,000$. Even as the number of points increases, the value doesn't deviate much from the continuum value.

Nonetheless, we aim to confirm that even when H is set to 100 and ρ is set to 2,000,000, the inclusion of higher order terms in the scalar curvature should improve the action for higher number of points which seems deviating for $N > 1000$ in Fig. (3.8). In the next chapter, we will provide a comprehensive explanation of the chain action which will encompass the quadratic component of curvature.

CHAPTER 4

HIGHER ORDER CORRECTION FOR CHAIN ACTION

To begin our correction of higher-order correction terms in the action, we examine Eq. (3.10). Within this equation, in order to focus solely on the linear term in R , it was assumed that $g^{\alpha\beta}g^{\mu\nu} = \eta^{\alpha\beta}\eta^{\mu\nu}$. Now, let's loosen this assumption and observe the consequences of doing so, keeping in mind that we are expanding the metric around a point (x_0, t_0) . We have,

$$\begin{aligned} R &= g^{\mu\nu}g^{\alpha\beta}R_{\alpha\mu\beta\nu} \\ &= (\eta^{\mu\nu} + \frac{1}{3}R_{\gamma\delta\epsilon\zeta}\eta^{\mu\delta}\eta^{\zeta\nu}x^\gamma x^\epsilon)(\eta^{\alpha\beta} + \frac{1}{3}R_{\gamma\delta\epsilon\zeta}\eta^{\alpha\delta}\eta^{\zeta\beta}x^\gamma x^\epsilon)R_{\alpha\mu\beta\nu}. \end{aligned} \quad (4.1)$$

Expanding all index contractions in this equation and keeping upto quadratic terms in the curvature, while noting that in two dimensions, the Riemann tensor has only one independent component characterized by R_{0101} , we obtain the following expression:

$$0 = R_{0101}^2((x - x_0)^2 - (t - t_0)^2) - 3R_{0101} - \frac{3}{2}R \quad (4.2)$$

Solving for R_{0101} using the quadratic equation gives

$$R_{0101} = \frac{3 \pm 3\sqrt{1 + \frac{2R[(x-x_0)^2 - (t-t_0)^2]}{3}}}{2[(x - x_0)^2 - (t - t_0)^2]} \quad (4.3)$$

Applying the binomial expansion and keeping upto quadratic terms in the scalar curvature, one of the roots of this quadratic equation can be expressed as

$$R_{0101} = -\left(\frac{R}{2} - \frac{R^2}{12}[(x - x_0)^2 - (t - t_0)^2]\right) \quad (4.4)$$

The line element in Eq. (3.9) will now have these components,

$$\begin{aligned}
g_{00} &= -1 + \frac{R}{6}(x - x_0)^2 - \frac{R^2}{36}((x - x_0)^2 - (t - t_0)^2)(x - x_0)^2 \\
g_{11} &= 1 + \frac{R}{6}(t - t_0)^2 - \frac{R^2}{36}((x - x_0)^2 - (t - t_0)^2)(t - t_0)^2 \\
g_{01} &= \frac{R}{6}(x - x_0)(t - t_0) - \frac{R^2}{36}((x - x_0)^2 - (t - t_0)^2)(x - x_0)(t - t_0) \\
g_{10} &= \frac{R}{6}(x - x_0)(t - t_0) - \frac{R^2}{36}((x - x_0)^2 - (t - t_0)^2)(x - x_0)(t - t_0)
\end{aligned} \tag{4.5}$$

and the line element will look like

$$\begin{aligned}
ds^2 &= \left(-1 + \frac{R}{6}(x - x_0)^2 - \frac{R^2}{36}((x - x_0)^2 - (t - t_0)^2)(x - x_0)^2 \right) dt^2 \\
&+ \left(1 + \frac{R}{6}(t - t_0)^2 - \frac{R^2}{36}((x - x_0)^2 - (t - t_0)^2)(t - t_0)^2 \right) dx^2 \\
&- \left(\frac{R}{6}(x - x_0)(t - t_0) - \frac{R^2}{36}((x - x_0)^2 - (t - t_0)^2)(x - x_0)(t - t_0) \right) (dtdx + dxdt)
\end{aligned} \tag{4.6}$$

As discussed in the previous section, it is crucial to modify the form of the line element (utilizing null coordinates (u, v)) in order to ensure that the metric takes on a conformally flat form. In order to achieve the appropriate coordinate transformation, we select a specific combination of $(v - v_0)^a$ and $(u - u_0)^b$ that maintains the dimensionality in quadratic term of Curvature. The key lies in determining the correct coefficient in the Eq. (4.7), which allows us to transform the metric into a conformally flat form.

$$\begin{aligned}
t &= \frac{u + v}{\sqrt{2}} + \frac{R}{12\sqrt{2}}((v - v_0)(u - u_0)^2 + (v - v_0)^2(u - u_0)) \\
&+ R^2(C(v - v_0)^2(u - u_0)^3 + D(v - v_0)^3(u - u_0)^2) \\
x &= \frac{u - v}{\sqrt{2}} + \frac{R}{12\sqrt{2}}((v - v_0)(u - u_0)^2 - (v - v_0)^2(u - u_0)) \\
&+ R^2(A(v - v_0)^2(u - u_0)^3 + B(v - v_0)^3(u - u_0)^2)
\end{aligned} \tag{4.7}$$

From these, we can derive the expressions for $(x^2, t^2, dx, dt, dx^2, dt^2, dxdt)$ in terms of the null coordinates (u, v) . By directly substituting these expressions into Eq. (4.6), we obtain the line

element of the form in Eq. (4.8). We are looking at the line element corresponding to the quadratic part in Eq. (4.8).

$$\begin{aligned}
ds^2 = & \frac{R^2}{48}(4u^3vdv^2 - 14u^2v^2dudv + 4uv^3du^2) \\
& + R^2\sqrt{2}\left[A(2v^3dudv - 2u^3vdv^2 + 3u^2v^2du^2 - 3u^2v^2dudv) \right. \\
& + B(3u^2v^2dudv - 3u^2v^2dv^2 + 2uv^3du^2 - 2uv^3dudv) \\
& + C(-2v^3dudv - 2u^3vdv^2 - 3u^2v^2du^2 - 3u^2v^2dudv) \\
& \left. + D(-3u^2v^2dudv - 3u^2v^2dv^2 - 2uv^3du^2 - 2uv^3dudv)\right]
\end{aligned} \tag{4.8}$$

By choosing

$$A = \frac{1}{48\sqrt{2}}, B = -\frac{1}{48\sqrt{2}}, C = \frac{1}{48\sqrt{2}}, D = \frac{1}{48\sqrt{2}} \tag{4.9}$$

The line element including the flat spacetime terms, R correction, and R^2 correction part can be reduced to

$$ds^2 = -(2 + R(v - v_0)(u - u_0) + \frac{13R^2}{24}(v - v_0)^2(u - u_0)^2)dudv. \tag{4.10}$$

Using the binomial expansion up to second order correction, we get

$$\sqrt{-g} = 1 + \frac{R}{2}(u - u_0)(v - v_0) + \frac{13R^2}{48}(u - u_0)^2(v - v_0)^2. \tag{4.11}$$

The volume of an Alexandrov set A in curved spacetime with interval (u_0, v_0) and (u_k, v_k) is given by

$$\begin{aligned}
V &= \int_A \sqrt{-g(u_k, v_k)} du_k dv_k \\
&= \int_{u_0}^{u_k} \int_{v_0}^{v_k} \left(1 + \frac{R}{2}(v_k - v_0)(u_k - u_0) + \frac{13R^2}{48}(u_k - u_0)^2(v_k - v_0)^2\right) du_k dv_k \\
&= (u_k - u_0)(v_k - v_0) + \frac{R}{8}(v_k - v_0)^2(u_k - u_0)^2 + \frac{13R^2}{432}(v_k - v_0)^3(u_k - u_0)^3.
\end{aligned} \tag{4.12}$$

Expression for V^{k-1} which is used during integration is given by

$$V^{k-1} = (u_k - u_0)^{k-1}(v_k - v_0)^{k-1} + \frac{R(k-1)}{8}(v_k - v_0)^k(u_k - u_0)^k + R^2(k-1)\left(\frac{13}{432} + \frac{k-2}{128}\right)(v_k - v_0)^{k+1}(u_k - u_0)^{k+1}. \quad (4.13)$$

We are now ready to calculate our chain distribution including second order correction terms starting with $\langle C_3 \rangle$.

4.1 $\langle C_3 \rangle$ including higher-order correction

We begin by integrating Eq. (3.3) for $k = 3$ including the R^2 term as follow,

$$\begin{aligned} \langle C_3 \rangle &= \rho_o \int_{A_0} \left(1 + \frac{R}{2}(v_3 - v_1)(u_3 - u_1) + \frac{13R^2}{48}(u_3 - u_1)^2(v_3 - v_1)^2\right) du_1 dv_1 \\ &\quad \rho_1 \int_{A_1} \left(1 + \frac{R}{2}(v_3 - v_2)(u_3 - u_2) + \frac{13R^2}{48}(u_3 - u_2)^2(v_3 - v_2)^2\right) du_2 dv_2 \end{aligned} \quad (4.14)$$

Continuing in a similar manner as demonstrated in Eq. (3.19), we arrive at this equation

$$\langle C_3 \rangle = \frac{N!}{V^2(N-2)!} \left[\frac{(u_3 - u_0)^2(v_3 - v_0)^2}{4} + \frac{5R}{72}(u_3 - u_0)^3(v_3 - v_0)^3 + \frac{157R^2}{6912}(u_3 - u_0)^4(v_3 - v_0)^4 \right] \quad (4.15)$$

Let's subtract and add $\left(\frac{R(u_3 - u_0)^3(v_3 - v_0)^3}{16} + \frac{131R^2(u_3 - u_0)^4(v_3 - v_0)^4}{6912}\right)$ and use $V^2 = (u_3 - u_0)^2(v_3 - v_0)^2 + \frac{R}{4}(u_3 - u_0)^3(v_3 - v_0)^3 + \frac{131R^2(u_3 - u_0)^4(v_3 - v_0)^4}{1728}$ from (4.13) to get

$$\langle C_3 \rangle = \frac{N!}{V^2(N-2)!} \left[\frac{V^2}{4} + \frac{R}{144}(u_3 - u_0)^3(v_3 - v_0)^3 + \frac{26R^2}{6912}(u_3 - u_0)^4(v_3 - v_0)^4 \right] \quad (4.16)$$

Now, using $R(u_3 - u_0)^3(v_3 - v_0)^3 = V^2 \left(\frac{RN}{\rho}\right) - \frac{3R^2}{8}(u_3 - u_0)^4(v_3 - v_0)^4$, we get

$$\langle C_3 \rangle = \frac{N!}{V^2(N-2)!} \left[\frac{V^2}{4} + \frac{V^2}{144} \left(\frac{RN}{\rho}\right) + \frac{R^2}{864}(u_3 - u_0)^4(v_3 - v_0)^4 \right] \quad (4.17)$$

Finally, using $R^2(u_3 - u_0)^4(v_3 - v_0)^4 = V^2 \left(\frac{RN}{\rho}\right)^2$, we arrive at the expression corresponding

to Eq. (3.21)

$$\langle C_3 \rangle = N(N-1) \left[\frac{1}{4} + \frac{1}{144} \frac{NR}{\rho} + \frac{1}{864} \left(\frac{NR}{\rho} \right)^2 \right] \quad (4.18)$$

Let's calculate for $\langle C_4 \rangle$ which will generate another quadratic equation similar to Eq. (4.18) and solve for R .

4.2 $\langle C_4 \rangle$ including higher-order correction

For $k = 4$, Eq. (3.3) with the higher order term to scalar curvature would look like as follows,

$$\begin{aligned} \langle C_4 \rangle = & \rho_o \int_{A_0} \left(1 + \frac{R}{2}(v_4 - v_1)(u_4 - u_1) + \frac{13R^2}{48}(u_4 - u_1)^2(v_4 - v_1)^2 \right) du_1 dv_1 \times \\ & \rho_1 \int_{A_1} \left(1 + \frac{R}{2}(v_4 - v_2)(u_4 - u_2) + \frac{13R^2}{48}(u_4 - u_2)^2(v_4 - v_2)^2 \right) du_2 dv_2 \times \\ & \rho_2 \int_{A_2} \left(1 + \frac{R}{2}(v_4 - v_3)(u_4 - u_3) + \frac{13R^2}{48}(u_4 - u_3)^2(v_4 - v_3)^2 \right) du_3 dv_3. \end{aligned} \quad (4.19)$$

Integrating (4.19) leads to

$$\langle C_4 \rangle = \frac{N!}{V^3(N-3)!} \left[\frac{(u_4 - u_0)^3(v_4 - v_0)^3}{36} + \frac{7R}{576}(u_4 - u_0)^4(v_4 - v_0)^4 + \frac{721R^2}{172800}(u_4 - u_0)^5(v_4 - v_0)^5 \right]. \quad (4.20)$$

Let's subtract and add $\left(\frac{3R(u_4 - u_0)^4(v_4 - v_0)^4}{288} + \frac{79R^2(u_4 - u_0)^5(v_4 - v_0)^5}{20736} \right)$ and use $V^3 = (u_4 - u_0)^3(v_4 - v_0)^3 + \frac{3R}{8}(u_4 - u_0)^4(v_4 - v_0)^4 + \frac{79R^2(u_4 - u_0)^5(v_4 - v_0)^5}{576}$ from (4.13) to get

$$\langle C_4 \rangle = \frac{N!}{V^3(N-3)!} \left[\frac{V^3}{36} + \frac{R}{576}(u_4 - u_0)^4(v_4 - v_0)^4 + \frac{47R^2}{129600}(u_4 - u_0)^5(v_4 - v_0)^5 \right]. \quad (4.21)$$

Now, using $R(u_4 - u_0)^4(v_4 - v_0)^4 = V^3 \left(\frac{RN}{\rho} \right) - \frac{R^2}{2}(u_4 - u_0)^5(v_4 - v_0)^5$, we get

$$\langle C_4 \rangle = \frac{N!}{V^3(N-3)!} \left[\frac{V^3}{36} + \frac{V^3}{576} \left(\frac{RN}{\rho} \right) - \frac{131R^2}{259200}(u_4 - u_0)^5(v_4 - v_0)^5 \right]. \quad (4.22)$$

Finally, using $R^2(u_4 - u_0)^5(v_4 - v_0)^5 = V^3 \left(\frac{RN}{\rho}\right)^2$ gives

$$\langle C_4 \rangle = N(N-1)(N-2) \left[\frac{1}{36} + \frac{1}{576} \frac{NR}{\rho} - \frac{131}{259200} \left(\frac{NR}{\rho}\right)^2 \right]. \quad (4.23)$$

4.3 Chain Action with higher-order correction

By solving Eq. (4.18) and Eq. (4.23), we can find R in terms of $\langle C_3 \rangle$ and $\langle C_4 \rangle$ as follows,

$$R = \frac{\rho}{N} \left[\frac{259200 \cdot \langle C_4 \rangle}{1236 \cdot N(N-1)(N-2)} + \frac{113184 \cdot \langle C_3 \rangle}{1236 \cdot N(N-1)} - \frac{35496}{1236} \right]. \quad (4.24)$$

The chain action is now given by

$$\begin{aligned} S &= \frac{N}{\rho} \cdot R \\ &= \left[\frac{259200 \cdot \langle C_4 \rangle}{1236 \cdot N(N-1)(N-2)} + \frac{113184 \cdot \langle C_3 \rangle}{1236 \cdot N(N-1)} - \frac{35496}{1236} \right]. \end{aligned} \quad (4.25)$$

The plot is given below

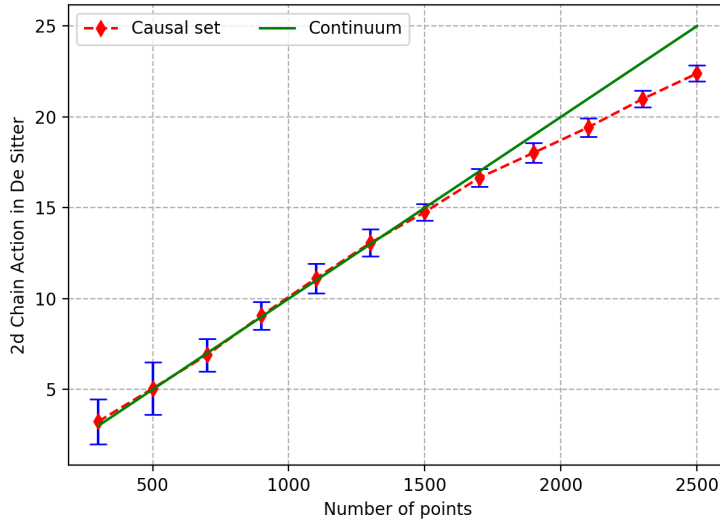


Figure 4.1: This graph is the chain action (S) when higher order terms in the scalar curvature are included. This is a result of averaging 50 different values of the causal set action for each N with $H = 100$ and $\rho = 2,000,000$.

Figure (4.1) shows that the error bars associated with the modified chain action are approximately of magnitude 1. These error bars progressively decrease as the number of data points increases. The modified version of the action appears to be highly precise until around $N = 1700$ points, after which it begins to deviate. If higher-order corrections such as (R^3, R^4, \dots) were included, the action value would be expected to converge towards the continuum even for higher number of points.

When compared to Dr. Pilgrim’s proposed chain action⁴, this modified version shows improved approximation to the continuum action, particularly for larger numbers of data points. This trend is depicted in the accompanying Fig. (4.2).

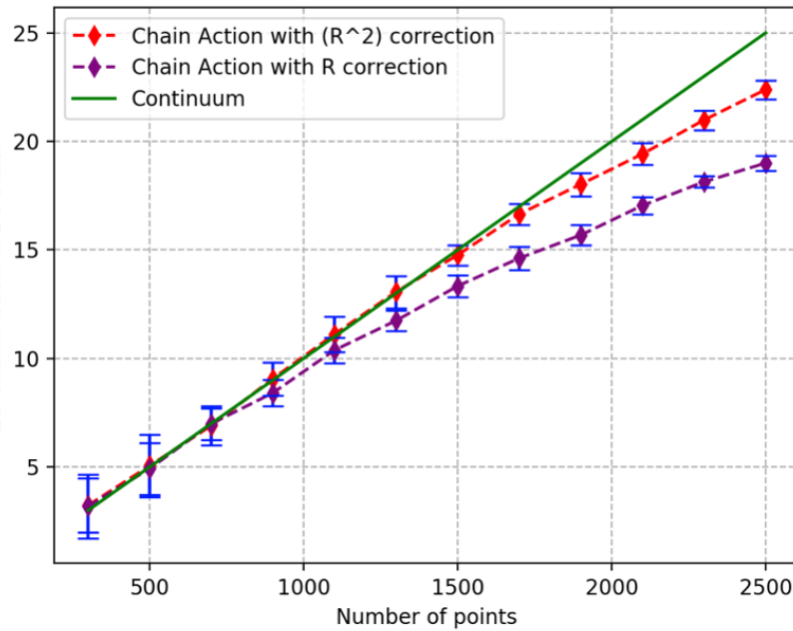


Figure 4.2: This graph presents a comparison between the chain action including only a linear curvature term (Eq. (3.21)) and the modified chain action that incorporates the R^2 term (equation 4.24).

Based on Fig. (4.2), it is evident that the modified chain action exhibits better convergence towards the continuum compared to the original chain action.

CHAPTER 5

CONCLUSION

The formulation of an Action is a significant advancement in causal set theory, playing a vital role in understanding the theory's evolution and dynamics. Despite the inherent non-local nature of causal sets, certain locally defined quantities such as the scalar curvature and Benincasa-Dowker (BD) Action were computed in the second chapter using a non-local discrete operator which depends on certain linear combination of layers. However, the resulting BD action failed to accurately match the continuum value and exhibited substantial statistical errors (in the order of $10^2 - 10^3$). A potential reason for this difference could be attributed to the fact that the Eq. (2.27) comprises terms originating directly from Poisson's distribution, which inherently results in higher uncertainties as the number of points increases. Another limitation may arise from ignoring higher order terms in the scalar curvature during the expansion of the metric.

Chapter 3 introduces an alternative approach proposed by Dr. BB and Dr. Bombelli, which explores the relationship between the expectation value of the k -chain length and the curvature. This method presents a more efficient approach and significantly reduces the error bars as the number of points increases, surpassing the performance of the BD method. However, the chain action still deviates from the continuum value with increasing point density (around 1000 points), possibly due to the ignorance of higher-order terms associated with the scalar curvature during the derivation.

The thesis in the fourth chapter focuses on investigating the enhancements of the chain action by incorporating higher-order terms of the scalar curvature during the expansion of the metric. Through extensive calculations, the specific form of the chain action, including these higher-order terms (specifically the R^2 term), in terms of $\langle C_3 \rangle$ and $\langle C_4 \rangle$, was successfully determined. The

result in Fig. (4.2) indicates that the chain action can be improved by incorporating higher-order terms associated with the scalar curvature.

LIST OF REFERENCES

1. Stanford Encyclopedia of Philosophy. Singularities and black holes, no date. URL <https://plato.stanford.edu/entries/spacetime-singularities/#toc>.
2. Sumati Surya. The causal set approach to quantum gravity. *Living Rev. Rel.*, 22(1):5, 2019. doi: 10.1007/s41114-019-0023-1.
3. Luca Bombelli, Jooan Lee, David Meyer, and Rafael D Sorkin. Space-time as a causal set. *Physical review letters*, 59(5):521, 1987.
4. Luca Bombelli and BB Pilgrim. A tale of two actions a variational principle for two-dimensional causal sets. *Classical and Quantum Gravity*, 38(8):085014, 2021.
5. Rafael D Sorkin. Does locality fail at intermediate length-scales. *Approaches to quantum gravity: Toward a new understanding of space, time and matter*, pages 26–43, 2009.
6. Dionigi Maria Teofilo Benincasa. *The action of a causal set*. PhD thesis, Imperial College London, 2013.
7. Jan Myrheim. Statistical geometry. Technical report, 1978.
8. Miremad Aghili. Manifoldlike causal sets. *Electronic Theses and Dissertations*, (1529), 2019. URL <https://egrove.olemiss.edu/etd/1529>.
9. Benjamin Pilgrim. Dynamics for discretized gravity in the causal set approach. *Electronic Theses and Dissertations*, (2128), 2021. URL <https://egrove.olemiss.edu/etd/2128>.
10. Santosh Bhandari. Exploring manifoldlike causal sets and their dimensions. *Honors Theses*, (1907), 2021. URL https://egrove.olemiss.edu/hon_thesis/1907.

APPENDICES

APPENDIX A

Mechanics of Sprinkling

As discussed in Ref. ¹⁰, To better understand the computational aspect of the two-dimensional Minkowski space, we can use a square manifold that contains an Alexandrov set extending from t_1 to t_2 along the time direction, and from $x_1 = (t_2 - t_1)/2$ to $x_2 = (t_1 - t_2)/2$ along the spatial direction. To distribute points in the manifold, we can choose the first value to be a time coordinate between t_2 and t_1 , and the second value to be a spatial coordinate between x_2 and x_1 . We then select only those points that are inside the Alexandrov set and assign them their respective locations. We repeat this process until we obtain the desired set of points.

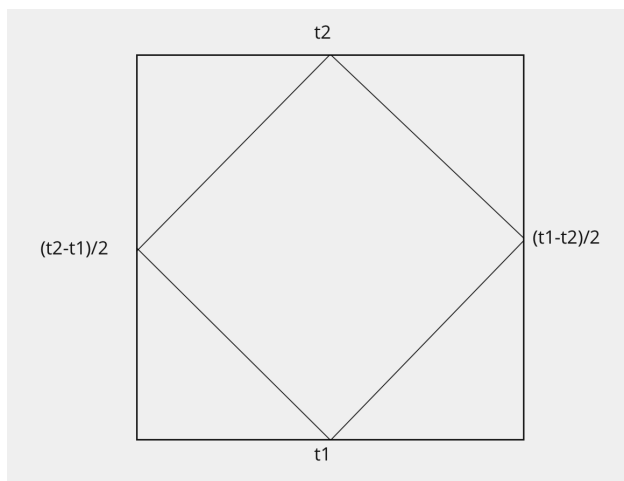


Figure A.1: Causal diamond inside a square Lorentzian manifold

For flat spacetime:

Line element: $ds^2 = -dt^2 + dx^2$

Volume element: $\sqrt{-g(x)}dxdt$

Since $\sqrt{-g(x)} = 1$, there is no dependence on t or x for the volume element in Minkowski space. Thus, we can choose points uniformly at random in both directions. Let's use computer's function to generate a random number r_t that can be translated to a random number m_t between t_1 and t_2 . They are related via equation below,

$$r_t = \frac{\int_{t_1}^{m_t} dt}{\int_{t_1}^{t_2} dt} \quad (\text{A.1})$$

where, $m_t \in [t_1, t_2]$ and $r_t \in [0, 1]$,

We can now generate m_t as a function of r_t given by

$$m_t = r_t(t_2 - t_1) + t_1 \quad (\text{A.2})$$

Similarly, the second coordinate (space) between x_1 and x_2 be m_x such that,

$$r_x = \frac{\int_{x_1}^{m_x} dt}{\int_{x_1}^{x_2} dt}, \quad (\text{A.3})$$

$$m_x = r_x(x_2 - x_1) + x_1$$

where, $m_x \in [x_1, x_2]$ and $r_x \in [0, 1]$.

Now that we have generated coordinates (m_t, m_x) randomly, we can determine if the generated points are in the diamond or not by satisfying this condition below,

$$\begin{aligned} (m_t - t_1)^2 &> (m_x)^2 \\ (m_t - t_2)^2 &> (m_x)^2 \end{aligned} \quad (\text{A.4})$$

This inequality checks if the generated points are timelike or not. In other words, it is checking if the points are causally related or not. We can, then, encode this information in a

partially ordered set using a relations or link matrix (also includes equivalent information), which can be arranged in lower or upper triangular form.

Relation matrix:

$$R_{ij} = \begin{cases} 1 & \text{if } i < j \\ 0 & \text{otherwise} \end{cases} \quad (\text{A.5})$$

If $< *$ defines the link relation between elements, then the Link matrix is,

$$L_{ij} = \begin{cases} 1 & \text{if } i < * j \\ 0 & \text{otherwise} \end{cases} \quad (\text{A.6})$$

For de Sitter space:

Line element:

$$ds^2 = \frac{1}{H^2 t^2} (-dt^2 + dx^2) \quad (\text{A.7})$$

where H = Expansion rate, $t \in (-\infty, 0)$ and $x \in (-\infty, \infty)$

Volume element:

$$dV = (H^2 t^2)^{-1} dx dt \quad (\text{A.8})$$

It is evident from the volume element that the volume depends on t , thus, we can't choose a uniformly random value m_t between t_1 and t_2 . For this reason, the density should be higher at the top of an Alexandrov set. However, the volume element is independent of x , thus, we can choose m_x uniformly between x_1 and x_2 .

For the time coordinate, let's choose m_t such that

$$r_t = \frac{\int_{t_1}^{m_t} (H^2 t^2)^{-1} dt}{\int_{t_1}^{t_2} (H^2 t^2)^{-1} dt} \quad (\text{A.9})$$

Let's express m_t in terms of r_t ,

$$m_t = \frac{t_2 t_1}{r_t (t_1 - t_2) + t_2} \quad (\text{A.10})$$

where $r_t \in [0, 1]$ and $m_t \in (t_1, t_2)$.

Since the volume element is independent of the x coordinate, it will behave in the same way it did in Minkowski space. So, we can write

$$m_x = r_x(x_2 - x_1) + x_1 \tag{A.11}$$

where $m_x \in [x_1, x_2]$ and $r_x \in [0, 1]$.

Now that we have generated (m_t, m_x) , we can use the same condition as we did in Minkowski space to determine if it belongs to the causal diamond or not. The only difference that will be observed is that the apparent density of points as we go higher on t appears to increase. The actual density is approximately equal to a constant.

VITA

Santosh Bhandari

Education

2021 - 2023 – **Master of Science (MS) in Physics** University of Mississippi
2017 - 2021 – **Bachelor of Science (BS) in Physics** University of Mississippi
THESIS: “Exploring Manifoldlike Causal Sets and their Dimensions”

Research Experience

2022 – 2023 – **Action in Causal Set Theory** University of Mississippi
2021 - 2022 – **Scalar Curvature for Causal Set Theory** University of Mississippi
2018 – 2021 – **Dimension for Causal Set Theory** University of Mississippi

Scholarships and Awards

2017–2021 – **Academic Excellence Scholarship** University of Mississippi
2020 – **Bolen Scholarship** University of Mississippi
2021 – **Best Poster Presentation at MAS** Biloxi, MAS
2020 – **Featured Undergraduate at UM homepage** University of Mississippi

Teaching Experience

2021–2023 – **Teaching Assistant for Astronomy lab** University of Mississippi
Summer 2023 – **Teaching Assistant for General Physics Lab** University of Mississippi